# Blood Pressure Dynamics During Simulated Ventricular Tachycardia in Patients After Right Ventricular Outflow Tract Reconstruction Mainly for Tetralogy of Fallot Compared With Patients After Ventricular Septal Defect Closure

Hideo Ohuchi, MD, Hiroyuki Ohashi, MD, Ken Watanabe, MD, Osamu Yamada, MD, Toshikatsu Yagihara, MD, and Shigeyuki Echigo, MD

We studied hemodynamic changes during simulated ventricular tachycardia using ventricular pacing. Hemodynamic deterioration during pacing is more significant in patients after right ventricular outflow tract reconstruction, especially in adults, than after closure of a ventricular septal defect. The cardiac autonomic nervous system has a significant impact on hemodynamics during simulated ventricular tachycardia. ©2004 by Excerpta Medica, Inc.

(Am J Cardiol 2004;93:1445–1448)

Late arrhythmias after definitive repair for congenital heart disease assume great importance, especially in adult patients[1] and are a major determinant of late morbidity and mortality.[2] Imbalance of cardiac autonomic nervous activity is a risk factor for arrhythmias, and baroreflex function has a significant role in arterial blood pressure (BP) recovery during ventricular tachycardia (VT) in adult patients.[3–5] Impaired baroreflex function is associated with symptoms and intolerance of tachyarrhythmia[6,7] and may cause hemodynamic deterioration and lethal ventricular fibrillation. Most postoperative patients with congenital heart disease exhibit abnormalities of the cardiac autonomic nervous system, especially impaired baroreflex function in complex anatomy patients.[8,9] This impairment may adversely influence hemodynamics during VT in these patients, who often also have residual hemodynamic abnormalities, causing volume and/or pressure overload. It is likely that the abnormal hemodynamics have a significant impact on BP change during VT. Because there are no studies addressing hemodynamics during tachyarrhythmias in patients with congenital heart disease, our purpose in the present study was to measure BP changes during ventricular pacing (simulated VT) and determine relations among BP changes, cardiac autonomic nervous activity, and hemodynamics at rest in patients with a history of right ventricular outflow tract reconstruction (RVOTR) for congenital heart disease.

From the Departments of Pediatrics and Thoracic Surgery, National Cardiovascular Center, Osaka, Japan. This work was supported by a grant from the Japan Cardiovascular Research Foundation, Osaka, Japan. Dr. Ohuchi's address is: Department of Physiology & Biophysics, Physiological Imaging Research Lab, Alfred Bldg. 2–404, Mayo Clinic, 200 1st Street SW, Rochester, Minnesota 55905. E-mail: ouchi.hideo@mayo.edu. Manuscript received December 9, 2003; revised manuscript received and accepted February 13, 2004.

• • •

We studied 29 patients with RVOTR (tetralogy of Fallot in 20, and other anomalies in 9) and 11 patients after closure of a ventricular septal defect (VSD). Of the patients with RVOTR, 16 were children and the others were adults; clinical and resting hemodynamic characteristics are shown in Table 1. Severe pulmonary regurgitation was present in 5 patients with tetralogy of Fallot. Diuretics and anticoagulants were given in 5 and 9 patients with RVOTR, respectively. No patients with RVOTR were receiving antiarrhythmic agents. No medications were given in postoperative patients with VSD. Of these patients, 9 patients had had an outlet VSD with right coronary cusp prolapse and 2 a perimembranous VSD with a significant shunt.

Heart rate variability and arterial baroreflex sensitivity were measured in all patients using previously reported methods.[8,9] The spectral heart rate variability was expressed as a low-frequency component (0.04 to 0.15 Hz) and a high-frequency component (0.15 to 0.40 Hz), and the logarithmic values, log (low-frequency component) and log (high-frequency component), were used. A bolus phenylephrine method was used to measure arterial baroreflex sensitivity (milliseconds/mm Hg).[10]

Cardiac catheterization was performed under light sedation to evaluate hemodynamics and ventricular function, including ventricular volume (divided by body surface area) and the ejection fraction.[8,9]

After hemodynamic evaluation, a 5Fr pacing catheter was positioned in the right ventricular outflow in all patients, ventricular pacing threshold was measured, and the heart paced at twice the pacing threshold. BP was directly recorded with a catheter inserted into the ascending aorta. Femoral venous pressure instead of central venous pressure was continuously recorded by way of a 7Fr sheath placed in the right femoral vein. Heart rate was derived from a continuous 6-lead electrocardiographic recordings.

After acceptable hemodynamic stability, the following protocol was used: (1) venous blood was taken from the femoral vein for plasma norepinephrine, (2) a rapid pacing rate at 150 beats/min for 1 minute, (3) venous blood sampling for plasma norepinephrine 15 seconds after the end of pacing, (4) recovery for 5 to 10 minutes, (5) rapid pacing rate at 180 beats/min for 1 minute, and (6) venous sampling for plasma norepi-



0002-9149/04/$–see front matter

doi:10.1016/j.amjcard.2004.02.055

TABLE 1 Clinical Characteristics of the Study Patients

| Variables | RVOTR | | VSD | |
|---|---|---|---|---|
| | Children (n = 16) | Adults (n = 13) | Children (n = 5) | Adults (n = 6) |
| Age (yrs) | 12 ± 2 | 22 ± 4 | 12 ± 1 | 21 ± 3 |
| Follow-up (yrs) | 7 ± 4 | 13 ± 5 | 1 ± 0 | 1 ± 0 |
| Central venous pressure (mm Hg) | 6 ± 3 | 6 ± 2 | 3 ± 0 | 4 ± 2 |
| Right ventricular pressure (mm Hg) | 55 ± 15 | 58 ± 17 | 25 ± 5 | 24 ± 9 |
| Right ventricular end-diastolic pressure (mm Hg) | 8 ± 1 | 9 ± 2 | 6 ± 1 | 5 ± 2 |
| Pulmonary artery pressure (mm Hg) | 17 ± 5 | 15 ± 3 | 13 ± 2 | 10 ± 4 |
| Right ventricular end-diastolic volume (ml/m$^2$) | 80 ± 20 | 102 ± 26* | 84 ± 17 | 71 ± 12 |
| Right ventricular ejection fraction (%) | 53 ± 8 | 53 ± 8 | 54 ± 4 | 54 ± 12 |
| Left ventricular end-diastolic pressure (mm Hg) | 10 ± 2 | 10 ± 2 | 10 ± 1 | 10 ± 5 |
| Left end-diastolic volume (ml/m$^2$) | 81 ± 15 | 102 ± 26* | 85 ± 22 | 73 ± 6 |
| Left ejection fraction (%) | 69 ± 9 | 59 ± 9* | 64 ± 7 | 65 ± 5 |
| Pulmonary resistance (U · m$^2$) | 2.5 ± 1.6 | 2.6 ± 0.7 | 1.6 ± 0.2 | 1.3 ± 0.6 |
| Systemic resistance (U · m$^2$) | 23 ± 5 | 31 ± 7* | 21 ± 6 | 24 ± 5 |
| Cardiac index (L/min/m$^2$) | 3.5 ± 0.8 | 2.7 ± 0.6* | 4.0 ± 0.7 | 3.3 ± 0.5 |

*p <0.01 vs. children (RVOTR).
Values are mean ± SD.

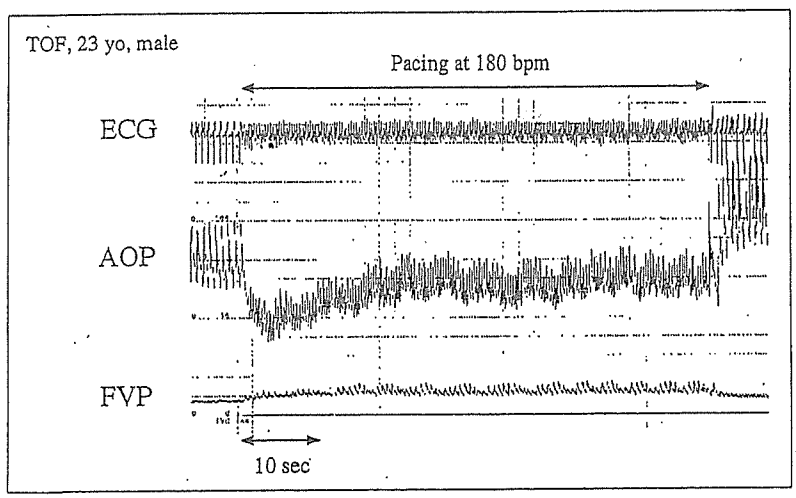


FIGURE 1. Sample tracing of surface elecrocardiogram, ascending aortic pressure (AOP), and femoral venous pressure (FVP) during 180 beats/min (bpm) ventricular pacing in a 23-year-old patient with tetralogy of Fallot (TOF).

TABLE 2 Comparison of Cardiac Autonomic Nervous Activity Among the Study Groups

| Variables | RVOTR | | VSD | |
|---|---|---|---|---|
| | Children | Adults | Children | Adults |
| Log (low-frequency component of heart rate variability) | 1.7 ± 0.7 | 1.8 ± 0.5 | 2.1 ± 0.3 | 2.0 ± 0.5 |
| Log (high-frequency component of heart rate variability) | 1.4 ± 0.5 | 1.6 ± 0.7 | 1.9 ± 0.5 | 1.9 ± 0.6 |
| Arterial baroreflex sensitivity (ms/mm Hg) | 6.4 ± 6.0 | 3.9 ± 3.5 | 12.2 ± 3.6 | 14.0 ± 4.1 |
| Plasma norepinephrine (pg/ml) | 185 ± 96 | 169 ± 72 | 212 ± 71 | 164 ± 119 |

Values are mean ± SD.

nephrine 15 seconds after the end of pacing. All patients tolerated the protocol. During pacing, the initial mean BP decrease from baseline to nadir (around initial the 10 seconds; Figure 1), mean BP recovery from nadir to steady state (last 10 seconds), and steady-state mean BP were measured. Plasma norepinephrine was determined by high-performance liquid chromatography.[11]

Informed consent was obtained from all subjects and/or their parents. The study protocol was approved by the ethical committee of the National Cardiovascular Center.

Differences in hemodynamics, cardiac autonomic nervous activity, and hemodynamic variables between the 2 study groups were evaluated using the unpaired *t* test, and differences in mean BP during pacing were assessed by repeated measures of analysis of variance. Simple linear regression analysis was used to evaluate correlations between mean BP changes and hemodynamics at rest, and cardiac autonomic nervous activity indexes and stepwise multivariate linear regression analysis were used to detect major determinants of the mean BP change during pacing. Data are expressed as the mean ± SD. A p value of $<0.05$ was considered statistically significant.

Hemodynamics were significantly impaired in the patients with RVOTR, especially the adults, compared with the patients with VSD (Table 1).

Although there was no difference in plasma norepinephrine, arterial baroreflex sensitivity, and log (high-frequency component) were lower in the patients with RVOTR. No difference in any cardiac autonomic nervous activity was observed between the child and adult patients with RVOTR or patients with VSD (Table 2).

In all groups, at the onset of pacing, BP decreased abruptly, whereas femoral venous pressure increased followed by a gradual increase in BP (BP recovery) with some fluctuations. At the end of pacing, all patients showed stable BP with small fluctuations (Figure 1). These hemodynamic changes were accompanied by an increase in plasma norepinephrine in the 2 RVOTR groups and the adult patients with VSD (Figures 2 and 3). Although no differences in mean BP change were observed between the RVOTR and VSD groups, the mean BP changes were greater during 180 pacing than 150 pacing ($p < 0.005$; Figures 2 and 3). Mean BP was

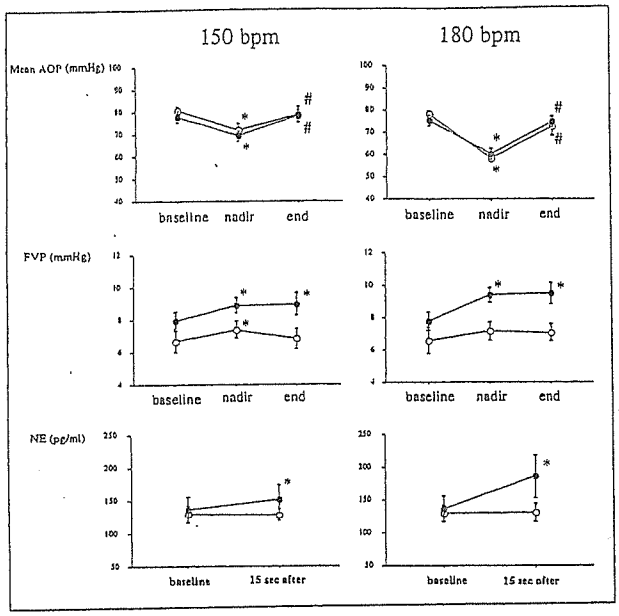


FIGURE 2. Changes in mean AOP, FVP, and plasma norepinephrine (NE) in children. *Open and closed circles,* patients after closure of VSD and those after RVOTR, respectively. *Significant versus baseline; #significant versus nadir. bpm = beats per minute; other abbreviations as in Figure 1.

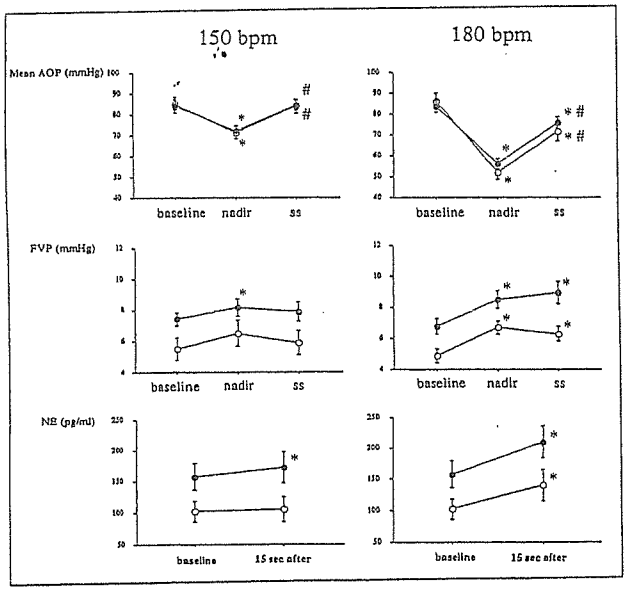


FIGURE 3. Changes in mean AOP, FVP, and plasma norepinephrine in adult patients. *Open and closed circles,* patients after closure of VSD and those after RVOTR, respectively. *Significant versus baseline; #significant versus nadir. ss = steady state; other abbreviations as in Figure 1.

greater in the adult patients than in the child patients, and, in adults, mean BP at 180 pacing was significantly lower than that at baseline.

Femoral venous pressure increased at the nadir of mean BP and tended to decrease at the end of pacing in the patients with VSD, resulting in no difference in the femoral venous pressure compared with baseline values, except for adult patients at 180 pacing. However, the femoral venous pressure at the end of pacing was significantly higher in the patients with RVOTR, except for the value at 150 pacing in adult patients (Figures 2 and 3). Plasma norepinephrine increased during both pacing periods in all patients with RVOTR; however, the increase was significant only in adult patients with VSD during 180 pacing (Figures 2 and 3).

In all patients, there was no correlation between plasma norepinephrine increase and mean BP recovery during 150 and 180 pacing. However, a significant positive relation was observed in all the adults ($r = 0.53$, $p < 0.05$) and it remained significant when the analysis was limited to adult patients with RVOTR (Figure 4).

In patients with RVOTR, high baseline mean BP was a major determinant for a greater initial mean BP decrease during 150 pacing and older age and higher baseline mean BP for the mean BP decrease during 180 pacing ($p < 0.001$ for each). Higher pulmonary artery and left ventricular end-diastolic pressures mainly determined the poor mean BP recovery during 150 pacing ($p < 0.01$), and high central venous pressure determined the poor mean BP recovery during 180 pacing ($p < 0.05$). Higher arterial baroreflex sensitivity and baseline mean BP were the major determinants for higher steady-state mean BP during 150 pacing (Figure 4), and higher baseline mean BP was the only determinant of higher mean BP at the end of 180 pacing ($p < 0.001$).

• • •

Our major findings are: (1) despite no difference in mean BP during pacing, responses of plasma norepinephrine and femoral venous pressure were greater in the patients with RVOTR; (2) faster pacing caused a greater initial mean BP decrease, and high baseline mean BP was a major determinant for a greater mean BP decrease and higher steady-state mean BP; (3) adult patients had a greater initial mean BP decrease; and (4) in addition to impaired hemodynamics, maintained arterial baroreflex sensitivity had a significant impact on higher steady-state mean BP during 150 pacing, and the sympathetic activation (plasma norepinephrine increase) was related to the mean BP recovery during faster pacing.

BP change during VT or ventricular pacing has been studied in dogs and adult patients with VT,[3–6,12] and the pacing site has little impact on hemodynamics during VT.[3,13] Faster VT rate and impaired left ventricular contractility are the main causes of hypotension during VT.[3] Our study confirms that the VT rate greatly impacts BP dynamics in patients with congenital heart disease. It is notable that the initial BP decrease was greater in adults than in children. Because BP is mainly determined by cardiac output and vascular resistance, a higher systemic arterial resistance may explain this finding; the systemic arterial resistance correlated well with the age of our patients with RVOTR ($r = 0.59$, $p < 0.001$).

Changes in femoral venous pressure and plasma norepinephrine were greater in the patients with RVOTR than in the patients with VSD despite no difference in BP during pacing. Increased tricuspid

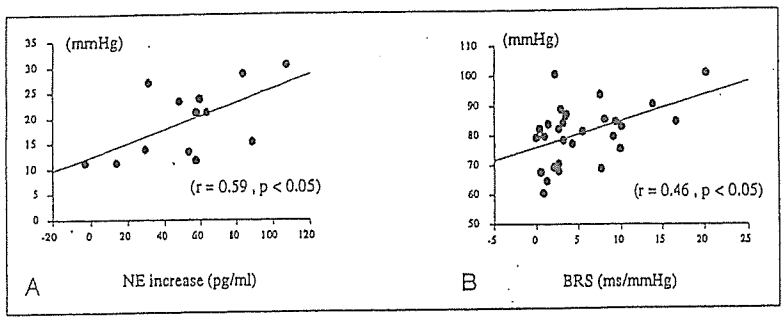


FIGURE 4. Relation between increase in plasma norepinephrine (NE) and AOP recovery during 180 beats/min ventricular pacing in adult patients with RVOTR *(A)* and that between arterial baroreflex sensitivity (BRS) and steady-state AOP during 150 beats/min ventricular pacing in all patients with RVOTR *(B)*. Other abbreviations as in Figure 1.

valve regurgitation similar to mitral valve regurgitation during VT[14] and a relative increase of the pressure gradient across right ventricular outflow tract may explain the femoral venous pressure increase. In addition, impaired positive force-frequency relations may cause hemodynamic deterioration,[15] because of the significantly lower ejection fraction in some adult patients with RVOTR.[16] The hemodynamic deterioration requires sympathetic activation, especially in adult patients with RVOTR, and this compensatory response may have unfavorable influences on sustaining VT. Because spontaneous termination of VT may be infrequent in patients with impaired baroreflex function,[17] evaluation of cardiac autonomic nervous activity would be beneficial and important in following these patients.

**Acknowledgment:** We are grateful to Peter M. Olley, MD, Adjunct Professor of Pediatrics, Sapporo Medical University, and Setsuko Olley, MD, for assistance in preparing the manuscript.

1. Wren C, O'Sullivan JJ. Survival with congenital heart disease and need for follow up in adult life. *Heart* 2001;85:438–443.
2. Gatzoulis MA, Balaji S, Webber SA, Siu SC, Hokanson JS, Poile C, Rosental M, Nakazawa M, Moller JH, Gillette PC, Webb GD, Redington AN. Risk factors for arrhythmia and sudden cardiac death late after repair of tetralogy of Fallot: a multicentre study. *Lancet* 2000;356:975–981.
3. Smith ML, Ellenbogen KA, Beightol LA, Eckberg DL. Sympathetic neural responses to induced ventricular tachycardia. *J Am Coll Cardiol* 1991;18:1015–1024.
4. Hamdan MH, Joglar JA, Page RL, Zagrodzky JD, Sheehan CJ, Wasmund SL, Smith ML. Baroreflex gain predicts blood pressure recovery during simulated ventricular tachycardia in humans. *Circulation* 1999;100:381–386.
5. Smith ML, Joglar JA, Wasmund SL, Carlson MD, Welch PJ, Hamdan MH, Quan K, Page RL. Reflex control of sympathetic activity during simulated ventricular tachycardia in humans. *Circulation* 1999;100:628–634.
6. Landolina M, Mantica M, Pessano P, Manfredini R, Foresti A, Achwarz PJ, De Ferrari GM. Impaired baroreflex sensitivity is correlated with hemodynamic deterioration of sustained ventricular tachycardia. *J Am Coll Cardiol* 1997;29:568–575.
7. van den Berg MP, Hassink RJ, Tuinenburg AE, Lefrandt JD, de Kam PJ, Crijns HJ. Impaired autonomic function predicts dizziness at onset of paroxysmal atrial fibrillation. *Int J Cardiol* 2001;81:175–180.
8. Ohuchi H, Suzuki H, Toyohara K, Tatsumi K, Ono Y, Arakaki Y, Echigo S. Abnormal cardiac autonomic nervous activity after right ventricular outflow tract reconstruction. *Circulation* 2000;102:2732–2738.
9. Ohuchi H, Takasugi H, Ohashi H, Okada Y, Yamada O, Yagihara T, Echigo S. Stratification of pediatric heart failure on the basis of neurohormonal and cardiac nervous activities in patients with congenital heart disease. *Circulation* 2003;108:2368–2376.
10. Smyth HS, Slight P, Pickering GW. Reflex regulation of arterial pressure during sleep in man. *Circ Res* 1969;24:109–121.
11. Mori K. Automated measurement of catecholamines in urine, plasma and hemogenates by high-performance liquid chromatography with fluorometric detection. *J Chromatogr* 1981;218:631–637.
12. Smith ML, Kinugawa T, Dibner-Dunlap ME. Reflex control of sympathetic activity during ventricular tachycardia in dogs: primary role of arterial baroreflexes. *Circulation* 1996;93:1033–1042.
13. Barold SS, Linhart JW, Hilder FJ, Samet P. Hemodynamic comparison of endocardial pacing of outflow and inflow tracts of the right ventricle. *Am J Cardiol* 1969;23:697–701.
14. Scully HD, Bello AG, Beierholm E, Frederiksen J, Weisfeldt ML, Daggett WM. The relationship between the atrial systolic-ventricular systolic interval and left ventricular function. *J Thorac Cardiovasc Surg* 1973;65:684–694.
15. Hasenfuss G, Holubarsch C, Hermann H-P, Astheimer K, Pieske B, Just H. Influence of the force-frequency relationship on haemodynamics and left ventricular function in patients with non-failing hearts and in patients with dilated cardiomyopathy. *Eur Heart J* 1994;15:164–170.
16. Waien SA, Liu PP, Ross BL, Williams WG, Webb GD, McLaughlin PR. Serial follow-up of adults with repaired tetralogy of Fallot. *J Am Coll Cardiol* 1992;20:295–300.
17. Waxman MB, Sharma AD, Cameron DA, Huerta F, Wald RW. Reflex mechanisms responsible for early spontaneous termination of paroxysmal supraventricular tachycardia. *Am J Cardiol* 1982;49:259–272.

# Abnormalities of Neurohormonal and Cardiac Autonomic Nervous Activities Relate Poorly to Functional Status in Fontan Patients

Hideo Ohuchi, MD; Hisashi Takasugi, MD; Hiroyuki Ohashi, MD; Osamu Yamada, MD; Ken Watanabe, MD; Toshikatsu Yagihara, MD; Shigeyuki Echigo, MD

*Background*—Impaired cardiac autonomic nervous activities and increased neurohumoral activities (CANA, NHA) characterize Fontan patients. However, the clinical significance of these changes is not clearly understood. Our purpose was to clarify the clinical significance of the CANA and NHA in stable Fontan patients.

*Methods and Results*—We divided 22 atriopulmonary connection (APC) and 75 total cavopulmonary connection (TCPC) patients into 4 subgroups according to New York Heart Association (NYHA) class (1.8±0.6) and measured various CANA and NHA indices. All NHA indices were elevated in the symptomatic patients ($P<0.001$). Natriuretic peptides were higher in the APC than in the TCPC patients, and the hemodynamics showed no correlation with brain natriuretic peptide in the APC patients. Low arterial oxygen saturation and impaired hemodynamics greatly influenced all elevated NHA indices ($P<0.01$), except for plasma renin activity, in the TCPC patients. Impaired CANA indices did not relate to NYHA class, although surgeries were associated with lower heart rate variability. In addition to poor correlation between NHA and CANA, age and ventricular morphology had no impact on all CANA and NHA indices, except for high norepinephrine in right ventricular Fontan patients.

*Conclusions*—Although symptomatic Fontan patients exhibit higher NHA, CANA is not related to either NYHA class or NHA. APC itself is responsible for higher natriuretic peptides, and arterial oxygen desaturation has a great impact on elevated NHA in the TCPC patients. These characteristics of the NHA and CANA differ from those of heart failure patients with biventricular physiology. (*Circulation.* **2004;110:2601-2608.**)

**Key Words:** Fontan procedure ■ heart defects ■ nervous system, autonomic ■ hormones ■ heart failure

Activated neurohumoral activity (NHA), impaired cardiac autonomic nervous activity (CANA), and low cardiac output and reduced exercise capacity characterize Fontan patients.[1–4] These changes resemble those in adult patients with chronic heart failure (CHF) and NHA and CANA have been useful in stratifying these adult CHF patients and predicting their prognosis.[5–10] These 2 indices are also, to some extent, applicable to postoperative patients with congenital heart disease after biventricular repair, especially in adult patients.[11] However, comprehensive evaluation of Fontan patients using NHA and CANA has not been undertaken. Our hypothesis was that relationships between these 2 indices and clinical status in Fontan patients with unique single-ventricular physiology might differ from those in biventricular physiology. In addition, we thought that the type of repair and ventricular morphology and surgery-related damage might influence these 2 indices. Therefore, the purpose of the present study was to measure various NHA and CANA indices and compare the results with clinical status, including hemodynamic and cardiopulmonary capacity.

## Methods

### Subjects

We studied prospectively 97 clinically stable Fontan patients (2 to 34 years old) and 48 control subjects. Clinical stability meant that patients were free from intravenous medications with no major change of oral medications, and the postoperative follow-up period was at least 4 months. Of the Fontan patients, a total cavopulmonary connection (TCPC) was created in 75 and an atriopulmonary connection (APC) in 22 (Table 1). All patients had undergone cardiac catheterization within the previous 1 year. Recently, our follow-up policy has included cardiac catheterization every 5 years after the operation to evaluate hemodynamics and exercise performance unless the patient had significant neurological or orthopedic complications. Of the present Fontan patients, there were no patients with sick sinus syndrome or possible renal dysfunction (creatinine >1.0). A patient with tricuspid atresia (20 years old) who had a ventricular tachycardia easily induced during exercise was excluded from the study. We divided our patients into 2 groups according to age <16 years (low-age group, 11±3 years old, n=63) and age ≥16 years (high-age group, 19±5 years old, n=34). Medications included digoxin (n=11), diuretics (n=49), anticoagulant agents (n=56), ACE inhibitors (n=8), antiarrhythmics (n=2), and

Received October 23, 2003; revision received March 9, 2004; accepted March 11, 2004.

From the Departments of Pediatrics (H. Ohuchi, H.T., H. Ohashi, O.Y., K.W., S.E.) and Thoracic Surgery (T.Y.), National Cardiovascular Center, Osaka, Japan.

Correspondence to Hideo Ohuchi (Ouchi), MD, Physiological Imaging Laboratory, Mayo Clinic, Al2-404, 200 1st St SW, Rochester, MN 55905. E-mail ouchi.hideo@mayo.edu



*Circulation* is available at http://www.circulationaha.org

DOI: 10.1161/01.CIR.0000145545.83564.51

TABLE 1. Subject Characteristics

| | Fontan | | | |
|---|---|---|---|---|
| NYHA Class | I | II | III+IV | Control |
| No. | 29 | 58 | 10 | 48 |
| Age, y | 14±4 | 14±6 | 14±4 | 15±4 |
| Height, cm | 152±18 | 145±16‡ | 144±25* | 159±16 |
| Weight, kg | 42±15* | 39±14‡ | 34±12† | 50±14 |
| Age at Fontan, y | 6±4 | 7±5 | 8±5 | ... |
| Follow-up, y | 8±4 | 8±4 | 6±4 | ... |
| Diagnosis | | | | |
| Isomerism | 9 | 14 | 7 | ... |
| TA | 8 | 18 | 1 | ... |
| UVH | 8 | 15 | 3 | ... |
| DORV | 6 | 10 | 3 | ... |
| MA | 3 | 7 | 2 | ... |
| PA | 4 | 1 | 0 | ... |
| Others | 0 | 7 | 1 | ... |
| Ventricular morphology | | | | |
| LV/BV/RV | 16/5/8 | 28/11/19 | 0/3/7 | 48/0/0 |
| Type of repair | | | | |
| APC | 6 | 14 | 2 | ... |
| IAR | 5 | 16 | 0 | ... |
| IAG | 14 | 19 | 5 | ... |
| ECR | 4 | 9 | 3 | ... |
| Previous or additional procedures at Fontan | | | | |
| APS | 16 | 36 | 7 | ... |
| PAB | 8 | 12 | 3 | ... |
| Glenn | 4 | 13 | 5 | ... |
| AVVP | 3 | 6 | 4 | ... |
| AAPA | 2 | 2 | 1 | ... |
| Fenestration | 1 | 2 | 2 | ... |
| Medications | | | | |
| Digoxin | 0 | 5 | 6 | ... |
| Diuretics | 11 | 29 | 9 | ... |
| Anticoagulant | 14 | 33 | 9 | ... |
| Antiarrhythmics | 0 | 1 | 1 | ... |
| Enalapril | 0 | 3 | 5 | ... |
| β-Blockers | 0 | 1 | 3 | ... |

AAPA indicates additional aortopulmonary anastomosis; APC, atriopulmonary connection; APS, aortopulmonary shunt; AVVP, atrioventricular valve plasty; BV, biventricle; DORV, double-outlet right ventricle; ECR, extracardiac rerouting; IAG, intracardiac grafting; IAR, intraatrial rerouting; LV, left ventricle; MA, mitral valve atresia; PA, pulmonary valve atresia; PAB, pulmonary artery banding; RV, right ventricle; TA, tricuspid valve atresia; and UVH; univentricular heart. Values are mean±SD.

*$P<0.05$, †$P<0.01$, ‡$P<0.001$ vs control.

β-blockers (n=4). The total number of surgical procedures including the Fontan operation ranged from 1 to 6 (mean, 2.6 operations per patient). Operations before the Fontan included systemic-to-pulmonary shunt(s) (n=59), pulmonary arterial banding (n=23), Glenn anastomosis (n=22), and atrioventricular valvuloplasty or valve replacement (n=13). Fenestration was created in 5 patients at the time of the Fontan operation and spontaneously closed in 2 patients 1 year after the operation. The age-matched control subjects were being followed up at our institute because of a history of coronary artery dilatation, aneurysm, or both because of Kawasaki disease, and all underwent follow-up selective coronary angiography to evaluate possible stenosis of the coronary arteries. Our control subjects showed no significant stenotic lesions of the coronary arteries.[1,5]

## Postoperative Status Based on New York Heart Association Classification

Because the New York Heart Association (NYHA) classification of cardiac status applies to adult cardiac patients, a modification of the classification was used for child patients.[12]

### Hemodynamics, Ventricular Morphology, and Calculation of Volume

Cardiac catheterization was performed in 95 patients and 46 control subjects within 1 week of exercise testing. We measured pressures in the cardiac chambers and great vessels. We estimated oxygen consumption from the age, sex, and heart rate (HR) and measured cardiac index ($L \cdot min^{-1} \cdot m^{-2}$) using the Fick principle with the assumption that right and left pulmonary arterial saturations were equal in patients with either a Glenn anastomosis or a TCPC, because it is clinically difficult to measure accurate flow distribution of the bilateral pulmonary arteries. Ventricular morphology was determined angiographically, and patients were divided into 3 groups,[1] ie, those with (1) a dominant left ventricle with or without a rudimentary right ventricle, (2) presence of both right and left ventricles, and (3) a dominant right ventricle with or without a rudimentary left ventricle. In this study, the groups consisted of 43, 19, and 35 patients, respectively. Patients with 2 ventricles in whom the volume of the smaller ventricle was either >30% of the main ventricle or was >50% of the predicted normal value were included in the biventricular group.[1] We used Simpson's rule to estimate morphological right and left ventricular volumes. End-diastolic ventricular volume was divided by body surface area to obtain end-diastolic volume index (EDVI), and systemic ventricular ejection fraction (EF) was calculated.[1,5]

### Neurohumoral Activities

After at least 15 minutes of supine rest, the plasma norepinephrine (NE) level,[13] atrial and brain natriuretic peptides (ANP, BNP), and renin activity (PRA) were determined in 95, 96, and 94 Fontan patients, respectively, and in all control subjects.[14–16] Plasma endothelin-1 (ET-1) was determined by radioimmunoassay in 62 Fontan patients and 22 control subjects.[17]

### Heart Rate Variability and Arterial Baroreflex Sensitivity

Heart rate variability (HRV) and arterial baroreflex sensitivity (BRS) were measured in 138 and 132 patients, respectively. The methods have been reported previously.[5] Briefly, after a 15-minute supine rest, ECG signals were recorded for 5 minutes, and beat-to-beat fluctuations were transformed into frequency domains by use of a fast Fourier transformation. The spectral HRV was expressed as a low-frequency (LF) component (0.04 to 0.15 Hz) and a high-frequency (HF) component (0.15 to 0.40 Hz), and the logarithmic values log LF and log HF were used. We used a bolus phenylephrine method to measure BRS (ms/mm Hg).[18]

### [$^{123}$I]Metaiodobenzylguanidine Scintigraphy

The methodology for this index was identical to that previously reported.[5] Metaiodobenzylguanidine (MIBG) scintigraphy was performed in 70 patients to evaluate myocardial adrenergic nervous activity. Myocardial images were acquired 4 hours after tracer injection, and the heart-to-mediastinal activity ratio (H/M) was calculated.

### Pulmonary Function Tests

We measured vital capacity (VC, in liters) and percent forced expiratory volume in 1 second in 134 patients (Spirosift, SP-600, Fukuda Denshi), and VC was calculated as the percentage of the body height–predicted normal value for our institute.

### Exercise Protocol

One hundred forty-two patients underwent symptom-limited treadmill exercise,[19] and peak oxygen uptake ($pV\dot{O}_2$) ($mL \cdot kg^{-1} \cdot min^{-1}$) and systolic blood pressure were measured and calculated as the percentage of body weight–predicted normal value for our institute. We used a 12-lead ECG to determine HR. Ventilation and gas exchange were measured by use of a breath-by-breath method using a hot-wire anemometer (Riko AS500, Minato Medical Science) with a mass spectrometer (MG-300, Perkin Elmer). Minute ventilation versus carbon dioxide production slope ($\dot{V}_E$-$\dot{V}CO_2$ slope) was determined and expressed as the percentage of our age- and sex-matched predicted normal values.

### Informed Consent

Informed consent was obtained from all patients and/or their parents. We asked control subjects and/or their parents to participate as volunteers. The Ethics Committee of the National Cardiovascular Center approved the study protocol.

### Statistical Analysis

Differences in hemodynamics, NHA, CANA, and exercise variables were evaluated using 1-way ANOVA with Bonferroni post hoc test. Univariate and stepwise multivariate linear regression analysis was used to detect independent determinants of CANA, NHA, and cardiopulmonary variables. Data are expressed as the mean±SD. A probability value of $P<0.05$ was considered statistically significant.

## Results

### NYHA Classification

The numbers of patients in the control and NYHA I, II, and III+IV categories were 48, 29, 58, and 10, respectively. Hemodynamics, NHA, CANA, and exercise variables for each category are shown in Table 2. Representative data according to NYHA classification are shown in the Figure.

### Hemodynamics

Low cardiac output was observed in proportion to functional severity, whereas a low EF with increased EDVI and elevated central venous and pulmonary artery pressures was present in NYHA III+IV. When symptomatic patients (NYHA II–IV) were compared with asymptomatic patients (NYHA I), there was no difference in any index between low- and high-age groups, except for a lower cardiac index in the high-age group ($P<0.05$) (Figure). Cardiac index was higher and arterial oxygen saturation ($Sao_2$) was lower in the TCPC than in the APC patients ($P<0.01$).

### Neurohumoral Activity

All NHA indices were elevated in proportion to functional capacity ($P<0.001$). BNP and NE in particular differentiated NYHA II from NYHA III+IV ($P<0.01$ to 0.001). Although all NHA indices were higher in the symptomatic patients than in the asymptomatic patients, no differences in these indices were observed between the asymptomatic patients and control subjects, except for ANP. Natriuretic peptides were higher in the APC than in the TCPC patients ($P<0.001$). There were no differences in NHA indices between low- and high-age groups.

### Cardiac Autonomic Nervous Activity

All CANA indices were markedly abnormal; however, they could not differentiate these patients on the basis of their functional classification, except for H/M in NYHA class III+IV. Moreover, there was no difference in CANA indices between symptomatic and asymptomatic patients, between low- and high-age groups, or between the APC and the TCPC patients.

TABLE 2. Hemodynamics, Neurohormonal and Cardiac Autonomic Nervous Activities, and Cardiopulmonary Variables According to NYHA Functional Status in Fontan Patients

| | | NYHA Class | | |
|---|---|---|---|---|
| Group | Control (n=48) | I (n=29) | II (n=58) | III+IV (n=10) |
| Hemodynamics | (n=46) | (n=29) | (n=57) | (n=10) |
| Central venous pressure, mm Hg | 3±1 | 11±3‡ | 12±3‡ | 14±4‡‖# |
| Pulmonary artery pressure, mm Hg | 13±2 | 10±2‡ | 11±3† | 13±4‖# |
| EDP, mm Hg | 11±2 | 7±3‡ | 8±3‡ | 9±4 |
| EF, % | 65±8 | 55±11‡ | 52±11‡ | 38±16‡¶‡‡ |
| EDVI, mL/m² | 80±15 | 77±20 | 79±27 | 115±47‡¶‡‡ |
| Cardiac index, L·min$^{-1}$·m$^{-2}$ | 3.6±0.6 | 2.7±0.7‡ | 2.4±0.6‡§ | 2.1±0.5‡§ |
| Arterial oxygen saturation, % | 98±1 | 95±2‡ | 95±3‡ | 90±8‡¶‡‡ |
| Neurohormonal activity | | | | |
| Norepinephrine, pg/mL | 158±71 | 205±76 | 256±130‡§ | 365±195‡¶†† |
| ANP, pg/mL | 20±10 | 45±45* | 68±53‡§ | 95±83‡‖ |
| BNP, pg/mL | 5±4 | 24±27 | 43±62‡ | 127±148‡¶‡‡ |
| PRA, ng·mL$^{-1}$·h$^{-1}$ | 3.0±2.2 | 5.3±3.2* | 8.3±11.1‡ | 12.1±8.2‡‖ |
| ET-1, pg/mL | 3.2±1.4 | 3.7±1.1 | 5.4±2.8†§ | 7.2±5.6‡‖ |
| Cardiac autonomic nervous activity | | | | |
| log LF | 2.6±0.4 | 1.7±0.5‡ | 1.5±0.6‡ | 1.5±0.4‡ |
| log HF | 2.5±0.5 | 1.4±0.6‡ | 1.2±0.5‡ | 1.3±0.6‡ |
| BRS | 17.5±5.9 | 3.8±3.5‡ | 3.0±3.0‡ | 1.9±2.2‡ |
| H/M | 2.9±0.5 | 1.8±0.3‡ | 1.7±0.4‡ | 1.4±0.5‡§ |
| Exercise variables | (n=48) | (n=29) | (n=56) | (n=9) |
| Peak $\dot{V}o_2$, % predicted | 96±13 | 60±8‡ | 50±7‡¶ | 36±6‡¶‡‡ |
| $\dot{V}E$-$\dot{V}co_2$ slope, % predicted | 99±13 | 125±21‡ | 135±24‡§ | 168±54‡¶‡‡ |
| Pulmonary function | (n=43) | (n=28) | (n=54) | (n=9) |
| Vital capacity, % predicted | 99±14 | 76±16‡ | 70±17‡ | 57±10‡‖# |
| Forced expired volume in 1 second, % | 91±8 | 89±6 | 88±7 | 86±9 |

ANP indicates atrial natriuretic peptide; BNP, brain natriuretic peptide; BRS, arterial baroreflex sensitivity; EDP, end-diastolic pressure; EF, ventricular ejection fraction; EDVI, end-diastolic volume index; H/M, heart-to-mediastinal metalodobenzylguanidine activity ratio; PV, pulmonary ventricle; SV, systemic ventricle; LF and HF, low- and high-frequency components of heart rate variability; and $\dot{V}E$-$\dot{V}co_2$ slope, ventilation versus bicarbon dioxide production slope.

*$P$<0.05, †$P$<0.01, ‡$P$<0.001 vs control; §$P$<0.05, ‖$P$<0.01, ¶$P$<0.001 vs I; #$P$<0.05, ††$P$<0.01, ‡‡$P$<0.001 vs II. Values are mean±SD.

## Vital Capacity

VC was small in all Fontan groups, especially in the III+IV patients, whereas their percent forced expiratory volume in 1 second was maintained. However, no significant difference in pulmonary function was observed between low- and high-age groups or between the APC and TCPC patients.

## Exercise Variables

Although there was no difference between the low- and high-age groups or the APC and the TCPC patients, p$\dot{V}o_2$ decreased and $\dot{V}E$-$\dot{V}co_2$ slope increased in proportion to NYHA classification ($P$<0.001).

## Correlation Between NHA and CANA

Relationships between NHA and CANA indices are shown in Table 3. NE correlated weakly with PRA and H/M. Natriuretic peptides and ET-1 correlated well with each other; however, relationships between NHA and CANA indices were either weak or nonexistent. BRS correlated closely with HRV, whereas no correlation between H/M and HRV or BRS was observed, except for log LF. Although NE, BNP, and ET-1 correlated inversely with p$\dot{V}o_2$, only H/M showed a weak positive correlation with p$\dot{V}o_2$.

## Multivariate Analysis

To determine the independent factors, the following parameters were used: age at tests and definitive repair, sex, follow-up period, number of surgeries, hemodynamics, VC, medications (diuretics), and exercise capacity (Table 4).

### *New York Heart Association*

High BNP and low EF were major determinants of low NYHA class in all Fontan patients ($P$<0.0001). When the TCPC patients were analyzed separately, ANP and EF were the major determinants of NYHA classification.

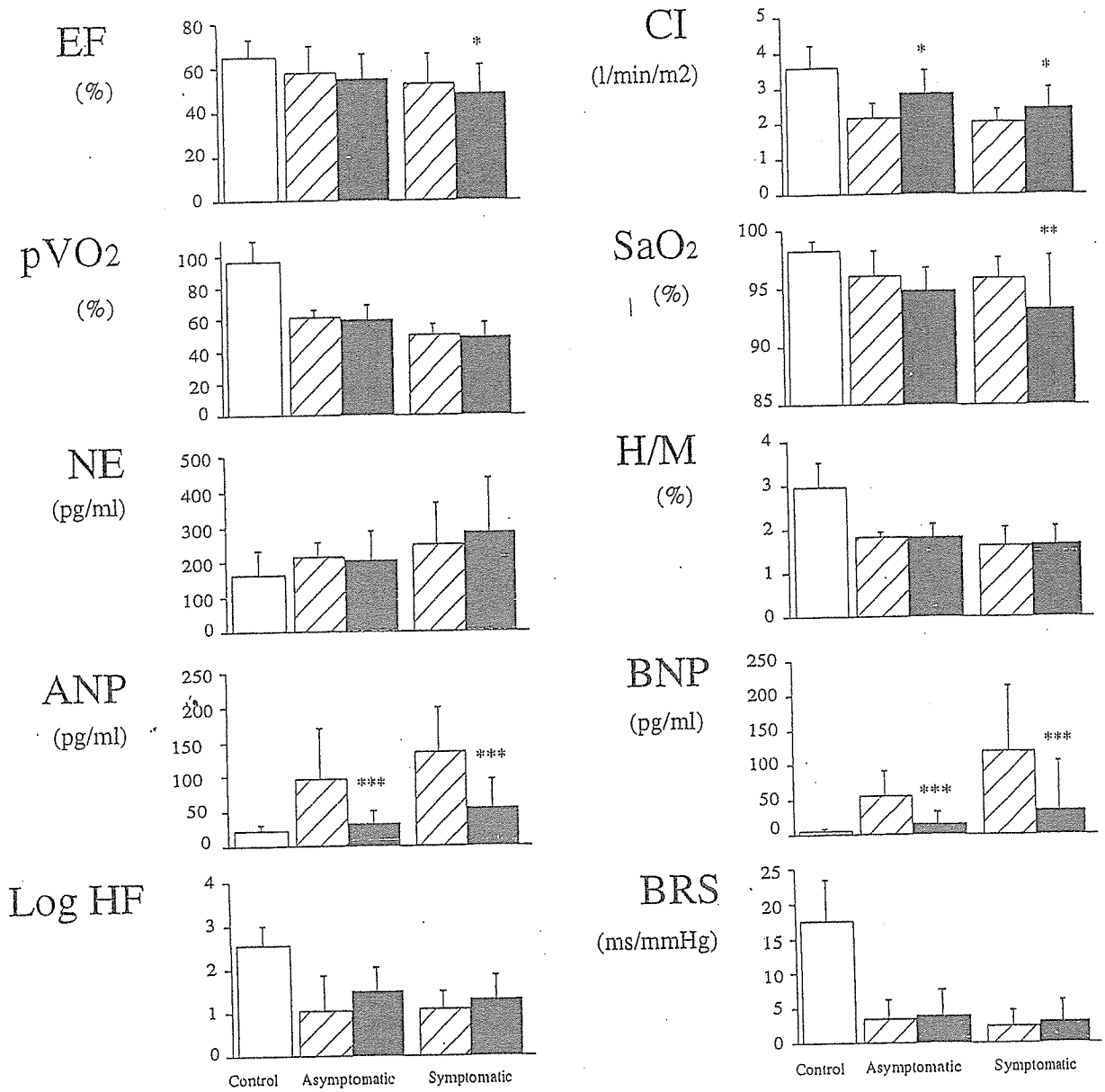


Relationship between categorized groups according to symptom-based classification and clinical variables. Abbreviations as in Table 2. CI indicates cardiac index. White, shaded, and black bars represent control subjects, APC, and TCPC patients, respectively. *$P<0.05$, **$P<0.01$, and ***$P<0.001$ versus APC patients.

*Neurohumoral Activity*

A high NE was determined by high age at operation and large EDVI ($P<0.01$). Both high natriuretic peptides were determined by the repair of APC, large EDVI, low $Sao_2$, and low cardiac output ($P<0.0001$). Male sex also determined high ANP. High PRA depended on the use of diuretics and low aortic blood pressure ($P<0.0001$) and high ET-1 on low cardiac output and low VC ($P<0.01$).

When the APC patients were analyzed, although low cardiac output and high ventricular end-diastolic pressure correlated with high ANP ($P<0.01$), no other indices were associated with high natriuretic peptides, except for use of diuretics for high PRA and ET-1 ($P<0.05$). When the TCPC patients were analyzed, high age at exercise and low $Sao_2$ correlated with high NE ($P<0.005$). Low $Sao_2$ also correlated with high natriuretic peptides and ET-1. In addition, low cardiac output and large EDVI were associated with high ANP and BNP, respectively. High PRA was determined by low arterial pressure and the use of diuretics ($P<0.0001$). Higher age at repair, short follow-up duration, and the use of diuretics were associated with high ET-1.

*Autonomic Nervous Activity*

A large number of surgical procedures, APC type repair, and low cardiac output correlated with low log LF and HF ($P<0.005$ for both). BRS was determined by low cardiac output and VC ($P<0.005$). Only the use of diuretics correlated with low H/M ($P<0.01$).

In APC patients, a high EDP correlated with a low BRS ($P<0.05$), and a low H/M was determined by a large number

TABLE 3. Correlation Coefficients Between Neurohumoral and Cardiac Autonomic Nervous Activities in Fontan Patients

| | Neurohormonal Activity | | | | | Cardiac Autonomic Nervous Activity | | | Exercise |
|---|---|---|---|---|---|---|---|---|---|
| | ANP | BNP | PRA | ET-1 | log LF | log HF | BRS | H/M | Peak $Vo_2$, % |
| Neurohormonal activity | | | | | | | | | |
| Norepinephrine | NS | NS | 0.23* | NS | NS | NS | NS | −0.33† | −0.37‡ |
| ANP | ... | 0.83‡ | NS | 0.50‡ | −0.21* | 0.25* | NS | NS | NS |
| BNP | ... | ... | NS | 0.58‡ | NS | NS | −0.21* | NS | −0.21* |
| PRA | ... | ... | ... | NS | NS | NS | NS | NS | NS |
| ET-1 | ... | ... | ... | ... | −0.34† | −0.35† | −0.40‡ | −0.40† | −0.42‡ |
| Cardiac autonomic nervous activity | | | | | | | | | |
| log LF | ... | ... | ... | ... | ... | 0.81‡ | 0.68‡ | 0.34† | NS |
| log HF | ... | ... | ... | ... | ... | ... | 0.59‡ | NS | NS |
| BRS | ... | ... | ... | ... | ... | ... | ... | NS | NS |
| H/M | ... | ... | ... | ... | ... | ... | ... | ... | 0.27* |

Abbreviations as in Table 2.
†$P<0.001$; ‡$P<0.0001$.

of surgical procedures and high central venous pressure ($P<0.001$). For the TCPC patients, only a large number of surgical procedures correlated with low HRV and BRS ($P<0.001$), whereas a longer follow-up period was associated with high H/M ($P<0.05$).

*Vital Capacity*

In addition to low $Sao_2$ and higher age at Fontan repair, a large number of surgical procedures correlated with a low VC ($P<0.0001$).

*$\dot{V}E$-$\dot{V}CO_2$ Slope*

High NE and low EF and $Sao_2$ correlated with a high $\dot{V}E$-$\dot{V}CO_2$ slope ($P<0.0001$).

## Subgroup Analysis

*Normal Versus Abnormal Natriuretic Peptides in NYHA I*

Of 29 Fontan patients in NYHA I, 9 and 14 patients showed high ANP (>40 pg/mL) and BNP (>13 pg/mL), respectively. However, no differences in cardiovascular reserve (peak HR, systolic blood pressure, $p\dot{V}O_2$, including VC) were observed between the high natriuretic peptide and the normal-range patients. The percentage of patients receiving diuretics was not different between the 2 groups.

*Influence of Ventricular Morphology on CANA and NHA*

NYHA class, EF, $Sao_2$, and $p\dot{V}O_2$ were lower and $\dot{V}E$-$\dot{V}CO_2$ slope was higher in the right ventricular type than the left ventricular type Fontan patients (Table 5, $P<0.05$ to 0.0001). However, ventricular morphology had no influence on the CANA or NHA indices, except for higher NE in the right ventricular type group ($P<0.05$).

## Discussion

We found that, in Fontan patients, (1) natriuretic peptides and EF were major determinants of NYHA status; (2) all NHA indices were elevated, although there was no difference between asymptomatic patients and control subjects; (3) APC

TABLE 4. Major Determinants and Their Standard β-Coefficients for Neurohumoral and Cardiac Autonomic Nervous Activities

| | | Surgery | | | Hemodynamics | | | | Medications | Lung | |
|---|---|---|---|---|---|---|---|---|---|---|---|
| Variables | Sex | Number | Age at Fontan | APC/TCPC | EDVI | MAO | $Sao_2$ | CI | Diuretics | VC | P |
| NE | | | 0.23 | | 0.22 | | | | | | <0.01 |
| ANP | −0.21 | | | −0.60 | 0.16 | | −0.27 | −0.26 | | | <0.0001 |
| BNP | | | | −0.52 | 0.24 | | −0.34 | −0.19 | | | <0.0001 |
| PRA | | | | | | −0.33 | | | 0.36 | | <0.0001 |
| ET-1 | | | | | | | | −0.37 | | −0.28 | <0.01 |
| log LF | | −0.35 | | 0.24 | | | | 0.24 | | | <0.001 |
| log HF | | −0.33 | | 0.26 | | | | 0.22 | | | <0.005 |
| BRS | | | | | | | | 0.29 | | 0.31 | <0.005 |
| H/M | | | | | | | | | −0.39 | | <0.005 |
| VC | | −0.68 | 0.17 | | | | 0.17 | | | ... | <0.0001 |
| $\dot{V}E/\dot{V}CO_2$ | | | | | | | −0.53 | | | | <0.0001 |

MAO indicates mean aortic pressure. Other abbreviations as in Table 2.

TABLE 5. Hemodynamics, Neurohormonal and Cardiac Autonomic Nervous Activities, and Cardiopulmonary Variables According to Systemic Ventricular Morphology

| Group | LV (n=43) | BV (n=19) | RV (n=35) |
|---|---|---|---|
| Age, y | 14±5 | 14±6 | 14±5 |
| NYHA class | 1.6±0.5 | 1.9±0.7 | 2.0±0.7† |
| APC/TCPC | 14/29 | 3/16 | 5/30 |
| Hemodynamics | | | |
| Central venous pressure, mm Hg | 11±3 | 12±3 | 12±3 |
| EF, % | 55±12 | 49±12 | 48±13* |
| Cardiac index, $L \cdot min^{-1} \cdot m^{-2}$ | 2.6±0.7 | 2.5±0.5 | 2.3±0.6 |
| Arterial oxygen saturation, % | 95±2 | 95±2 | 93±5* |
| Neurohormonal activity | | | |
| Norepinephrine, pg/mL | 228±121 | 234±112 | 291±148* |
| ANP, pg/mL | 72±62 | 51±48 | 61±52 |
| BNP, pg/mL | 52±70 | 38±60 | 44±85 |
| Cardiac autonomic nervous activity | | | |
| log HF | 1.2±0.6 | 1.3±0.7 | 1.3±0.5 |
| BRS | 2.9±3.3 | 3.7±3.2 | 3.0±3.0 |
| H/M | 1.7±0.3 | 1.7±0.5 | 1.7±0.4 |
| Exercise variables | | | |
| Peak $\dot{V}o_2$, % predicted | 56±8 | 50±12* | 48±10‡ |

LV, BV, and RV indicate left, biventricular, and right ventricular type ventricle as a systemic ventricle, respectively. Other abbreviations as in previous tables. Values are mean±SD.

*$P<0.05$, †$P<0.01$, ‡$P<0.001$ vs LV.

itself was responsible for high natriuretic peptides, and decreased $Sao_2$ had a great impact on the elevated NHA in the TCPC patients; and (4) although cardiac surgeries were related to CANA, impaired CANA had no influence on NHA or NYHA status.

## Neurohormonal Activities

Bolger et al[20] described the clinical use of NHA to stratify adult patients with congenital heart disease. However, it is not clear whether the relationship between NHA abnormalities and functional status applies to Fontan patients because of the wide variety of their diseases. Our study demonstrates that stratification based on the abnormal NHA is less significant in Fontan patients than has been reported in biventricular physiology patients, although symptomatic patients exhibit a high NHA. In fact, we could not find any difference in hemodynamics and cardiovascular reserve between asymptomatic patients with elevated NHA and those without. APC itself, rather than the hemodynamics, has a great impact on higher natriuretic peptides and ET-1. An increased secretion of BNP and ANP from the hypertrophied atrial myocardium in the APC patients may be responsible for the high natriuretic peptides.[21] Interestingly, $Sao_2$ has a significant impact on the elevated NHA in the TCPC patients. Resting (and maybe exercise-induced) decreased $Sao_2$ also causes sympathetic nervous activation[22] and excess ventilation,[23] and these are related to poor prognosis in adult heart failure patients.[10] Moreover, in addition to sympathetic dominant CANA,[24] high natriuretic peptides may worsen the Fontan patients' hypercoagulable state because of their diuretic effect.[25] The mechanism responsible for high ET-1 is unidentified in the present study, but the low pulmonary arterial oxygen saturation because of low cardiac output in addition to nonpulsatile flow may be an explanation.[26] The presence of a low systemic blood pressure and the use of diuretics imply that the renin-angiotensin system is important to maintaining perfusion pressure in these patients.

## Cardiac Autonomic Nervous Activity

CANA indices are prognostic guides in patients after myocardial infarction[8] and with heart failure.[9,27] However, the benefit of HRV in severe patients may be slight,[28] and this is especially true in Fontan patients because of their severely impaired CANA.[11] In addition, the lack of a relationship between CANA and exercise capacity also makes clinical classification difficult. In contrast to biventricular patients,[11] the prolonged lack of reinnervation after the Fontan procedure may explain the absence of a difference in CANA indices between child and adult patients.[5] In addition to the influence of surgical technique, low cardiac output is associated with a lower HRV and BRS and high NHA; consequently, maintaining a good cardiac output is important in patients with Fontan physiology. Alternatively, the Fontan circulation per se may cause a low H/M, because even the NYHA I patients without significant elevation in NE showed a low value, and no correlation between surgical procedures and H/M was observed. The reason why the use of diuretics had a significant impact on the low H/M, as observed in the biventricular patients, is unclear in the present study.[11]

## Exercise Variables and VC

Exercise capacity by definition determines the NYHA classification. VC distinguished the asymptomatic from the symptomatic patients, and the $\dot{V}E/\dot{V}Co_2$ slope identified relatively severe patients.[29] Mismatched ventilation-perfusion in the lung and elevated dead space ventilation have been considered to be major determinants of the excess ventilation in Fontan patients. However, the significant arterial desaturation also has a great impact on the excess ventilation in these patients, as demonstrated in the present study.

## Clinical Implications

Although natriuretic peptides and ventricular function stratify patients in line with their NYHA classification, we should be aware of the discrepancy between NHA and functional status, especially the lack of relationship between BNP and EF in the APC patients and the decreased sensitivity of NHA and CANA for detecting a reduced cardiovascular capacity. These present results imply that the diagnostic information from NHA and CANA indices cannot be applied to Fontan patients in the same manner as for patients with biventricular physiology.[11]

Nevertheless, considering the many clinical findings in adult cardiac patients, the abnormal physiological and biochemical findings in Fontan patients, even when they are asymptomatic, imply that they have a poor prognosis and suggest the need for treatment for these patients. In addition to congenitally determined factors (ventricular morphology,

function of the atrioventricular valve) and surgery-associated issues such as age at operation, functional status (NYHA class) is a possible determinant of their poor long-term prognosis.[30] In this respect, nonsurgical interventions that focus on maintaining physical fitness through exercise training and medication to prevent deterioration in EF and NHA are rational. Furthermore, we need to follow the unique contributions of NHA and CANA to the long-term prognosis in these patients.

### Study Limitations

Although we focused on Fontan patients, their surgical procedures varied from patient to patient. In addition, the structural anatomic variability in our study population is marked. However, a prospective randomized trial in these patients is clinically difficult and would require a very large number of patients. Another limitation is that our control subjects are not entirely normal; microangiitis may exist even when there is no apparent radiographic abnormality, and this may influence CANA or NHA or both.

## Acknowledgments

We are grateful to Drs Peter M. Olley, Adjunct Professor of Pediatrics, Sapporo Medical University, and Setsuko Olley for assistance in preparing the manuscript.

## References

1. Ohuchi H, Yasuda K, Hasegawa S, et al. Influence of ventricular morphology on aerobic exercise capacity in patients after the Fontan operation. *J Am Coll Cardiol.* 2001;37:1967–1974.
2. Ohuchi H, Tasato H, Sugiyama H, et al. Responses of plasma norepinephrine and heart rate during exercise in patients after Fontan operation and patients with residual right ventricular outflow tract obstruction after definitive reconstruction. *Pediatr Cardiol.* 1998;19:408–413.
3. Stewart JM, Seligman KP, Zeballos G, et al. Elevated atrial natriuretic peptide after the Fontan procedure. *Circulation.* 1987;76(suppl III):III-77–III-82.
4. Driscoll DJ, Danielson GK, Puga FJ, et al. Exercise tolerance and cardiorespiratory response to exercise after the Fontan operation for tricuspid atresia or functional single ventricle. *J Am Coll Cardiol.* 1986;7:1087–1094.
5. Ohuchi H, Hasegawa S, Yasuda K, et al. Severely impaired cardiac autonomic nervous activity after the Fontan operation. *Circulation.* 2001;104:1513–1518.
6. Cohn JN, Levine TB, Olivari MT, et al. Plasma norepinephrine as a guide to prognosis in patients with congestive heart failure. *N Engl J Med.* 1984;311:819–823.
7. Berger R, Huelsman M, Strecker K, et al. B-type natriuretic peptide predicts sudden death in patients with congestive heart failure. *Circulation.* 2002;105:2392–2397.
8. La Rovere MT, Bigger JT Jr, Marcus FI, et al. Baroreflex sensitivity and heart rate variability in prediction of total cardiac mortality after myocardial infarction. ATRAMI (Autonomic Tone and Reflex After Myocardial Infarction) Investigators. *Lancet.* 1998;351:478–484.
9. Blichick KC, Fetics B, Djoukeng R, et al. Prognostic value of heart rate variability in chronic congestive heart failure (Veterans Affairs' Survival Trial of Antiarrhythmic Therapy in Congestive Heart Failure). *Am J Cardiol.* 2002;90:24–28.
10. Ponikowski P, Francis DP, Piepoli MF, et al. Enhanced ventilatory response to exercise in patients with congestive heart failure and preserved exercise tolerance: marker of abnormal cardiopulmonary reflex control and predictor of poor prognosis. *Circulation.* 2001;103:967–972.
11. Ohuchi H, Takasugi H, Ohashi H, et al. Stratification of pediatric heart failure on the basis of neurohormonal and cardiac autonomic nervous activities in patients with congenital heart disease. *Circulation.* 2003;108:2368–2376.
12. Bruns LA, Chrisant MK, Lamour JM, et al. Carvedilol as therapy in pediatric heart failure: an initial multicenter experience. *J Pediatr.* 2001;138:505–511.
13. Mori K. Automated measurement of catecholamines in urine, plasma and homogenates by high-performance liquid chromatography with fluorometric detection. *J Chromatogr.* 1981;218:631–637.
14. Hama N, Nakao K, Mukoyama M, et al. Fundamental and clinical evaluation of "SHINORIAR ANP" human atrial natriuretic peptide IRMA kit. *Clin Report.* 1991;25:455–462.
15. Kono M, Yamaguchi A, Tsuji T, et al. An immunoradiometric assay for brain natriuretic peptide in human plasma. *Kaku Igaku.* 1993;13:2–7.
16. Ikeda I, Iinuma K, Takai M, et al. Measurement of plasma renin activity by a simple solid phase radioimmunoassay. *J Clin Endocrinol Metab.* 1982;54:423–428.
17. Ando K, Hirata Y, Shichiri M, et al. Presence of immunoreactive endothelin in human plasma. *FEBS Lett.* 1989;245:164–166.
18. Smyth HS, Slight P, Pickering GW. Reflex regulation of arterial pressure during sleep in man. *Circ Res.* 1969;24:109–121.
19. Ohuchi H, Nakajima T, Kawade M, et al. Measurement and validity of the ventilatory threshold in patients with congenital heart disease. *Pediatr Cardiol.* 1996;17:7–14.
20. Bolger AP, Sharma R, Li W, et al. Neurohormonal activation and the chronic heart failure syndrome in adults with congenital heart disease. *Circulation.* 2002;106:92–99.
21. Inoue S, Murakami Y, Sano K, et al. Atrium as a source of brain natriuretic polypeptide in patients with atrial fibrillation. *J Card Failure.* 2000;6:92–96.
22. Halliwill JR, Minson CT. Effect of hypoxia on arterial baroreflex control of heart rate and muscle sympathetic nerve activity in humans. *J Appl Physiol.* 2002;93:857–864.
23. Sietsema KE, Cooper DM, Perloff JK, et al. Control of ventilation during exercise in patients with central-to-systemic arterial shunts. *J Appl Physiol.* 1988;64:234–242.
24. von Kanel R, Dimsdale JE. Effects of sympathetic activation by adrenergic infusions on hemostasis in vivo. *Eur J Haematol.* 2000;65:357–369.
25. Hokins WE, Hall C. Paradoxical relationship between N-terminal proatrial natriuretic peptide and filling pressure in adults with cyanotic heart disease. *Circulation.* 1997;96:2215–2220.
26. Nootens M, Kaufmann E, Rector T, et al. Neurohormonal activation in patients with right ventricular failure from pulmonary hypertension: relation to hemodynamic variables and endothelin levels. *J Am Coll Cardiol.* 1995;26:1581–1585.
27. Merlet P, Valette H, Dubois-Rande JL, et al. Prognostic value of cardiac metaiodobenzylguanidine imaging in patients with heart failure. *J Nucl Med.* 1992;33:471–477.
28. Makikallio TH, Huikuri HV, Hintze U, et al. Fractal analysis and time- and frequency-domain measures of heart rate variability as predictors of mortality in patients with heart failure. *Am J Cardiol.* 2001;87:178–182.
29. Gitt AK, Wasserman K, Kilkowski C, et al. Exercise anaerobic threshold and ventilatory efficiency identify heart failure patients for high risk of early death. *Circulation.* 2002;106:3079–3084.
30. Driscoll DJ, Offord KP, Feldt RH, et al. Five-to fifteen-year follow-up after Fontan operation. *Circulation.* 1992;85:496–496.

# Role of Calcineurin B Homologous Protein in pH Regulation by the $Na^+/H^+$ Exchanger 1: Tightly Bound $Ca^{2+}$ Ions as Important Structural Elements†

Tianxiang Pang,‡ Takashi Hisamitsu,‡ Hidezo Mori,⊥ Munekazu Shigekawa,§ and Shigeo Wakabayashi*,‡

‡Department of Molecular Physiology and Department of Cardiac Physiology, National Cardiovascular Center Research Institute, Suita, Osaka 565-8565, Japan, and Department of Human Life Sciences, Senri Kinran University, Suita, Osaka 565-0873, Japan

Received November 10, 2003; Revised Manuscript Received January 27, 2004

ABSTRACT: We studied the role of the interaction of calcineurin homologous protein 1 (CHP1) with the $Na^+/H^+$ exchanger 1 (NHE1), particularly its EF-hand $Ca^{2+}$ binding motifs, in the intracellular pH ($pH_i$)-dependent regulation of NHE1. We found that $^{45}Ca^{2+}$ binds to two EF-hand motifs (EF3 and 4) of the recombinant CHP1 proteins with high affinity (apparent $K_d$ = ~90 nM). Complex formation between CHP1 and the CHP1 binding domain of NHE1 resulted in a marked increase in the $Ca^{2+}$ binding affinity ($K_d$ = ~2 nM) by promoting a conformational change of the EF-hands toward the tightly $Ca^{2+}$-bound form. This suggests that CHP1 always contains two $Ca^{2+}$ ions when associated with NHE1 in cells. Interestingly, overexpression of GFP-tagged CHP1 with mutations in EF3 or EF4 significantly reduced the exchange activity in the neutral $pH_i$ range and partly impaired the activation of NHE1 in response to various stimuli, such as growth factors and osmotic stress. Furthermore, we found that, in addition to reducing the activity ($V_{max}$), a CHP1 binding-defective NHE1 mutant had a marked reduction in $pH_i$ sensitivity (~0.7 pH unit acidic shift), which consequently abolished various regulatory responses of NHE1. These observations suggest that the association of NHE1 with CHP1 is crucial for maintenance of the $pH_i$ sensitivity of NHE1 and that tightly bound $Ca^{2+}$ ions may serve as important structural elements in the "$pH_i$ sensor" of NHE1.

The $Na^+/H^+$ exchanger (NHE1[1]) proteins in the plasma membrane and various organellar compartments of mammalian cells catalyze the electroneutral countertransport of $Na^+$ for $H^+$. Nine distinct isoforms of the $Na^+/H^+$ exchanger (NHE1 to NHE9) have been isolated to date, and these molecules have been shown to exhibit similar membrane topologies with 12 predicted N-terminal membrane-spanning helices and a large C-terminal cytoplasmic region (*1*−*10*). They show considerable differences in their tissue expression patterns, membrane localization, and kinetic and pharmacological properties. The plasma membrane exchangers (NHE1−5) are primarily involved in regulation of intracellular pH and $Na^+$ concentration, but they also participate in a broad range of physiological processes, such as cell volume regulation, transepithelial transport of electrolytes, cell proliferation, apoptosis, and differentiation (*1*−*3*).

Of the nine isoforms identified to date, NHE1 has been characterized in the most detail. NHE1 is ubiquitously expressed in essentially all tissues and cell types and plays a major role in maintaining intracellular pH and cell volume homoeostasis. The activity of NHE1 is controlled by various extrinsic factors, including growth factors, hormones, and mechanical stimuli (*1*−*3*). A variety of signaling molecules regulate the NHE1 protein, such as calcinuerin B homologous protein (CHP) (*11*−*13*), $Ca^{2+}$/calmodulin (*14*, *15*), the low molecular weight GTPases Ras and Rho (*16*), p42/44 mitogen-activated protein kinases (*17*), p90 ribosomal S6 kinase (*18*), 14-3-3 protein (*19*), Nck-interacting kinase (*20*), phosphatidylinositol 4,5-bisphosphate (*21*), and carbonic anhydrase II (*22*). Recently, we have focused on the role of CHP in regulation of the activities of the $Na^+/H^+$ exchangers (*12*, *13*).

CHP was initially discovered as a protein (p22) involved in vesicular transport (*23*), as well as a molecule that interacted with NHE (*11*). Since then, CHP has been reported

† This work was supported by Grant-in-Aid for Priority Areas 13142210 and Grant-in-Aid 14580664 for Scientific Research from the Ministry of Education, Science, and Culture of Japan, by the promotion of Fundamental Studies in Health Science of the Organization for Pharmaceutical Safety and Research of Japan (Promotion of Fundamental Studies in Health Science), and by Grant nano-001 for Research on Advanced Medical Technology from the Ministry of Health, Labor, and Welfare of Japan. T.P. was supported by a Japan Society for the Promotion of Science Postdoctoral Fellowship.

* To whom correspondence should be addressed. Department of Molecular Physiology, National Cardiovascular Center Research Institute, Fujishirodai 5-7-1, Suita, Osaka 565-8565 Japan. Tel: +81-6-6833-5012. Fax: +81-6-6835-5314. E-mail: wak@ri.ncvc.go.jp.

‡ Department of Molecular Physiology, National Cardiovascular Center Research Institute.

⊥ Department of Cardiac Physiology, National Cardiovascular Center Research Institute.

§ Senri Kinran University.

[1] Abbreviations: NHE, $Na^+/H^+$ exchanger; CHP, calcineurin B homologous protein; GFP, green fluorescent protein; CaN, calcineurin; CaM, calmodulin; $pH_i$, intracellular pH; EIPA, 5-(*N*-ethyl-*N*-isopropyl)-amiloride; DMEM, Dulbecco's modified Eagle's medium; HEPES, 2-[4-(2-hydroxyethyl)-1-piperazinyl]ethansulfonic acid; Tris, Tris(hydroxymethyl)aminomethane; EGTA, *O*,*O*′-bis(2-aminoethyl)ethylene glycol-*N*,*N*,*N*′,*N*′-tetraacetic acid; PBS, phosphate-buffered saline; PDGF-BB, platelet-derived growth factor-BB, PMA, phorbol 12-myristate 13-acetate; SDS−PAGE, sodium dodecyl sulfate−polyacrilamide gel electrophoresis.

10.1021/bi0360004 CCC: $27.50 
Published on Web 03/06/2004

to exhibit multiple functions, including inhibition of calcinuerin phosphatase activity (*24*), as well as interaction with microtubules (*25*), DRAK2 (death-associated protein kinase related apoptosis inducing protein kinase 2) (*26*) and KIF1Bβ2 (kinesin-family 1Bβ2) (*27*). Previously, we reported that the ubiquitous CHP isoform (designated as CHP1) is an essential cofactor for the physiological activity of the $Na^+/H^+$ exchanger by interacting with the juxtamembrane region in the C-terminal cytoplasmic domain of plasma membrane exchanger isoforms (*12*). Furthermore, we reported that the second CHP isoform (CHP2) might be involved in maintenance of the abnormally high $pH_i$ in malignantly transformed cells (*13*). CHP2 is expressed at a relatively high level in the rat small intestine (*28*), suggesting that it plays a specific role in this tissue. These CHP proteins contain four EF-hand $Ca^{2+}$ binding motifs and are myristoylated at the N-terminus ($Gly^2$). In addition, CHP1 is phosphorylated in cells in a serum-dependent manner (*11*). However, the roles of these posttranslational modifications of CHP proteins in the $pH_i$-dependent regulation or acute activation of NHE in response to extracellular stimuli are largely unknown, although this protein family appears to be essential for the physiological exchange activity of plasma membrane NHEs.

In this study, we focused on the EF-hand $Ca^{2+}$ binding motifs of CHP1. We found that the affinity of CHP1 for $Ca^{2+}$ markedly (approximately 40-fold) increases upon complex formation with NHE1, probably by promoting a change in the conformation of the EF-hand motifs. The extremely low $Ca^{2+}$ dissociation constant (~2 nM) of CHP1 suggests that $Ca^{2+}$ ions remain tightly bound to CHP1 when it is complexed with NHE1 in the plasma membrane. On the basis of properties of various CHP1 and NHE1 mutant proteins in cells, we suggest that CHP1 is important for $pH_i$-dependent regulation of NHE1 and that tightly bound $Ca^{2+}$ ions play an important role in maintaining a structure that is critical for this function of CHP1.

## EXPERIMENTAL PROCEDURES

*Materials.* The amiloride derivative EIPA was a gift from the New Drug Research Laboratories of Kanebo, Ltd. (Osaka, Japan). $^{45}CaCl_2$, $^{22}NaCl$, and $^{14}C$-benzoic acid were purchased from Dupont-NEN (Boston, MA). The rabbit polyclonal antibodies against CHP1 and NHE1 were described previously (*12*, *14*). All other chemicals were of the highest purity available.

*Cells, Culture Conditions, and Stable Expression.* The exchanger-deficient cell line PS120 (*29*) and corresponding transfectants were maintained in DMEM (Life Technologies Inc., Rockville, MD) containing 25 mM $NaHCO_3$ and supplemented with 7.5% (v/v) fetal calf serum, penicillin (50 units/mL), and streptomycin (50 μg/mL). Cells were maintained at 37 °C in the presence of 5% $CO_2$. PS120 cells ($5 \times 10^5$ cells/100-mm dish) were transfected with each plasmid construct (20 μg) by the calcium phosphate coprecipitation technique. Cell populations stably expressing wild-type or mutant human NHE1 were selected by the $H^+$-killing procedure as described previously (*30*). Cells stably overexpressing GFP-tagged CHP1 were first selected with G418, and then single colonies were selected by monitoring GFP fluorescence.

*Construction of Expression Vectors.* All the constructs were produced by means of a polymerase chain reaction (PCR)-based strategy. For construction of GFP-tagged CHP1 or its mutant forms with mutations in $Ca^{2+}$ binding motifs or in the myristoylated glycine (G2A), a cDNA encoding CHP1 was cloned into the mammalian expression vector pEGFP-N1 (Clontech, Palo Alto, CA). The plasmids carrying cDNAs for the wild-type or mutant NHE1s were all cloned into the mammalian expression vector pECE. Constructs were confirmed by sequencing plasmids with an ABI-PRISM DNA sequencer model 3100 (Applied Biosystems, Foster City, CA).

*Purification of Recombinant Proteins.* Recombinant histidine-tagged CHP1 proteins were produced in *Escherichia coli* (BL21-Star; Invitrogen, San Diego, CA) transformed with pET11 carrying the cDNA encoding CHP1 containing the C-terminal six histidine residues as described previously (*12*). Myristoylated CHP1 was produced using the same bacteria except they also contained the vector pBB131, which carries the yeast *N*-myristoyltransferase cDNA (kindly provided by Dr. J. I. Gordon, Washington University). Myristoylation of CHP1 (or p22) produced by this method was previously confirmed (*23*). For production of the complex of CHP1 and the CHP1 binding region of NHE1, the cytoplasmic region (aa 503−545) of NHE1 was cloned into the vector pET24 and coexpressed with His-tagged CHP1 in *E. coli* in the presence of ampicillin and kanamycin. Myristoylated and nonmyristoylated CHP1 proteins and CHP1/NHE1 (aa 503−545) complex proteins were all recovered in the soluble fraction and partially purified by passage through a $Ni^{2+}$ affinity resin column (ProBond, Invitrogen) according to the manufacturer's protocol. Partially purified CHP1 proteins were found to be ~70% pure. We did not carry out further purification of CHP1 because of aggregation during storage. The complexes consisting of CHP1 or its mutant variants complexed with the NHE1 fragment were further purified to more than 95% by diethylaminoethyl-Sepharose column chromatography. All the proteins were dialyzed overnight against 60 mM KCl and 10 mM HEPES/Tris (pH 7.2).

*Measurement of Equilibrium $^{45}Ca^{2+}$ Binding.* $^{45}Ca^{2+}$ binding to the proteins was measured by a filtration method as described previously (*31*). Purified proteins (0.1−0.2 mg/mL) were incubated for 1 h at 25 °C in a solution containing 60 mM KCl, 5 mM $MgCl_2$, 50 μM $CaCl_2$, 0.02 μCi/mL $^{45}CaCl_2$, 10 mM HEPES/Tris (pH 7.2), and different concentrations of EGTA (0−58 mM), giving a free $Ca^{2+}$ concentration of 0.1 nM to 50 μM. Aliquots (1 mL) of the reaction mixture were transferred onto 0.22-μm Millipore filters (Millipore, Bedford, MA) and filtered under vacuum. As controls, the same reaction mixtures without proteins were filtered to measure the background binding of $^{45}Ca$ by the filters. More than 95% of the proteins were retained in the filters. After the filters were dried, $^{45}Ca$ radioactivity was measured by scintillation counting.

*Measurement of $^{45}Ca^{2+}$ Release from Proteins.* $^{45}Ca^{2+}$ release from proteins was measured using a rapid filtration apparatus as described previously (*31*). After preincubation of proteins with a solution containing 50 μM $^{45}CaCl_2$ for 1 h, aliquots (1 mL) of reaction mixtures were filtered through Millipore filters. Filters were washed at a constant rate (0.2−2 mL/s) for the indicated periods (0.2−30 s) with

0.4−6 mL of 60 mM KCl, 5 mM $MgCl_2$, 10 mM HEPES/Tris (pH 7.2), and 10 mM EGTA. After the filters were dried, $^{45}Ca$ radioactivity was measured by scintilation counting.

*Immunoprecipitation and Immunoblotting.* Immunoprecipitation and immunoblotting were performed essentially as described previously (*14*). Briefly, cells were solubilized with 1% Triton X-100 in a solution of 150 mM NaCl, 10 mM HEPES-Tris (pH 7.4), and protease inhibitors. Cell lysates were incubated with respective antibodies and protein A Sepharose. After centrifugation, precipitated materials were separated on 7.5% or 12% polyacrylamide gels and electrophoretically transferred to Immobilon membranes (Millipore). After blocking, incubation with antibodies and washing, protein signals were visualized by enhanced chemiluminescence (Amersham, Buckinghamshire, U.K.). The signal intensity was measured using a photonic microscope system (ARUGUS-100, Hamamatsu photonics).

*Measurement of $^{22}Na^+$ Uptake.* $^{22}Na^+$ uptake activity and its $pH_i$ dependence were measured by the $K^+$/nigericin $pH_i$ clamp method essentially as described previously (*32*). Serum-depleted cells in 24-well dishes were incubated for 30 min at 37 °C in $Na^+$-free choline chloride/KCl medium containing 20 mM HEPES/Tris (pH 7.4), 1.2−140 mM KCl, 2 mM $CaCl_2$, 1 mM $MgCl_2$, 5 mM glucose (or 5 mM 2-deoxyglucose plus 2 μg/mL oligomycin under conditions of ATP depletion), and 5 μM nigericin. $^{22}Na^+$ uptake was started by adding the same choline chloride/KCl solution containing $^{22}NaCl$ (37 kBq/mL, final concentration = 1 mM), 1 mM ouabain, and 100 μM bumetanide. In some wells, 0.1 mM EIPA was added to the solution. After 1 min, cells were washed four times with ice-cold PBS to terminate $^{22}Na^+$ uptake. The $pH_i$ was calculated from the imposed $K^+$ concentration gradient by assuming the equilibrium $[K^+]_i/[K^+]_o = [H^+]_o/[H^+]_i$ and an intracellular $K^+$ concentration of 120 mM. Data were normalized according to the protein concentration as measured by the bicinchoninic assay (Pierce Chemical Co., IL) using bovine serum albumin as a standard.

*Measurement of $pH_i$.* Changes in $pH_i$ were measured by the [$^{14}$C]-benzoic acid equilibration method (*30*). For this measurement, serum-depleted cells were incubated for 30 min in bicarbonate-free HEPES-buffered DMEM (pH 7.0) and then incubated in the same medium containing [$^{14}$C]-benzoic acid (37 kBq/mL) for 20 min at 37 °C. After the cells were washed four times with ice-cold PBS, $^{14}$C-radioactivity taken up by cells was measured. Changes in $pH_i$ were calculated as described previously (*30*).

*Statistics.* Data of the pH dependence of EIPA-sensitive $^{22}Na^+$ uptake were simulated by fitting the values to the sigmoidal dose-response equation, rate of EIPA-sensitive $^{22}Na^+$ uptake = $V_{max}/(1 + 10^{\log(pK - pH_i)n})$ ($pK$ = $pH_i$ giving half-maximal $^{22}Na^+$ uptake; $n$ = Hill coefficient), using the simulation program included in Graphpad Prizm (Microsoft Corp., Redmond, WA). Equilibrium $^{45}Ca^{2+}$ binding was fitted to the dose−response equation, $^{45}Ca^{2+}$ bound = maximal $^{45}Ca^{2+}$ bound/$(1 + (K_d - [Ca^{2+}])^n)$ ($K_d$ = apparent dissociation constant for $Ca^{2+}$; $n$ = Hill coefficient). Kinetic parameters were expressed as the best fit values with standard errors, whereas other data were expressed as the means ± SD for at least three determinations.

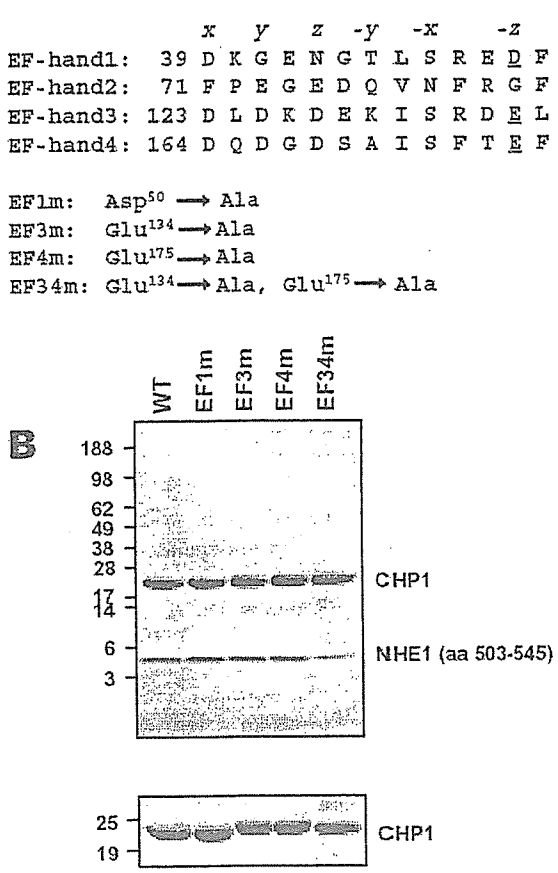


FIGURE 1: Amino acid sequences of EF-hand motifs and purified proteins of various CHP1 mutants. Panel A shows amino acid sequences of four EF-hand motifs present in CHP1. In four mutant CHP1s (EF1m, EF3m, EF4m, and EF34m), $Asp^{50}$, $Glu^{134}$, $Glu^{175}$, and both $Glu^{134}$/$Glu^{175}$ were replaced by alanine. In panel B, the purified complex of His-tagged CHP1 with the NHE1 segment (aa 503−545) (10 μg) was separated by electrophoresis on a 4−15% gradient (upper panel) or 12% SDS−PAGE gel (lower panel) and then visualized by Coomassie Brilliant Blue staining.

## RESULTS

*Characterization of $Ca^{2+}$ Binding Motifs in CHP1.* We first analyzed $^{45}Ca^{2+}$ binding to EF-hand motifs of CHP1 using recombinant CHP1 and its complex with the binding domain in NHE1. CHP1 interacts with NHE1 at the juxtamembrane region of the carboxyl-terminal cytoplasmic domain of NHE1. Hydrophobic residues of NHE1, such as $Phe^{526}$, $Leu^{527}$, $Leu^{530}$, and $Leu^{531}$, were shown to be important for the interaction of CHP1 with NHE1 (*12*). CHP1 contains four potential EF-hand $Ca^{2+}$ binding motifs, of which two ancestral sites (EF1 and -2) may not bind $Ca^{2+}$ due to substitution of critical acidic residues (Figure 1A). The canonical EF-hand consists of 29 consecutive residues with two flanking helices and a 12-residue loop (Figure 1A). The chelating loop residues in positions 1 (+$x$), 3 (+$y$), 5 (+$z$), 7 (−$y$), 9 (−$x$), and 12 (−$z$) ligate $Ca^{2+}$ through seven oxygen atoms arranged three-dimensionally on the axes of a pentagonal bipyramid (*33*, *34*). The −$z$ position, providing the only side chain oxygen atoms, is crucial for $Ca^{2+}$ binding (*33*−*35*). To characterize these $Ca^{2+}$ binding motifs, we introduced mutations into EF1, -3, and -4 in which acidic residues (aspartic acid or glutamic acid) at the −$z$ position were replaced by alanine (Figure 1B). We coexpressed the wild-type or mutant CHP1s together with the juxtamembrane region of NHE1 (aa 503−545) in *E. coli*. We confirmed that

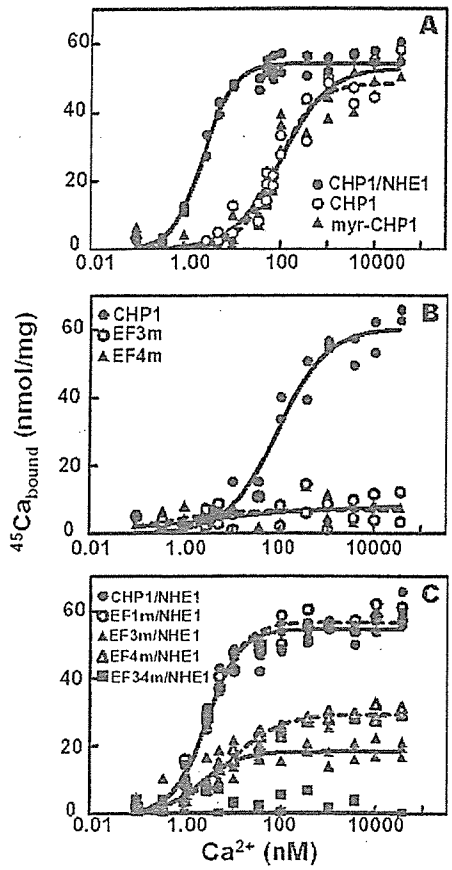


FIGURE 2: Equilibrium $^{45}Ca^{2+}$ binding to various CHP1 mutant proteins. In panels A−C, CHP1 or its various mutant proteins and the complex of CHP1 variants with the NHE1 segment (aa 503−545) (0.1−0.2 mg/mL) were incubated for 1 h in solutions containing 50 $\mu$M $^{45}CaCl_2$ and various concentrations of EGTA, which produce 0.2 nM to 50 $\mu$M free $Ca^{2+}$. Symbols corresponding to each protein variant were indicated in figures. The solutions were filtered through Millipore filters, and $^{45}Ca^{2+}$ bound to the CHP1 proteins was measured.

the purified complex proteins (>95% pure) of the wild-type CHP1, EF1m, EF3m, or EF4m with aa 503−545 of NHE1 were retained as a single peak on gel filtration chromatography and contained the CHP1 variant and the NHE1 peptide at a 1:1 molar ratio (data not shown). In addition, using 4−15% polyacrylamide gradient gels, we confirmed that the purified samples mostly contained comparable molar amounts of the CHP1 variant and the NHE1 fragment (Figure 1B, upper panel). However, in EF34m with double mutations at EF3 and -4, the amount of the NHE1 fragment was significantly reduced, suggesting that this double mutation impairs the interaction of CHP1 with NHE1. On 12% SDS−PAGE, EF3m, EF4m, and EF34m proteins were found to migrate more slowly than the wild-type or EF1m proteins (Figure 1B, lower panel), suggesting that a mutation-induced conformational change occurred in these three mutant proteins that had impaired $Ca^{2+}$ binding (see below).

We measured $^{45}Ca^{2+}$ binding to various CHP1 mutant proteins by a membrane filtration procedure. We found that $^{45}Ca^{2+}$ bound to the partially purified CHP1 proteins with an apparent $K_d$ of ~90 nM (Figure 2A and Table 1). The maximal amount of $^{45}Ca^{2+}$ bound to CHP1 corresponded to ~2 mol of $Ca^{2+}$ bound/mol of CHP1, assuming that the CHP1 sample was 70% pure. Myristoylation did not significantly affect the apparent affinity for $Ca^{2+}$ nor the

Table 1: Parameters for Equilibrium $^{45}Ca^{2+}$ Binding

| proteins | apparent $K_d$ ± SE (nM)[a] | Hill coefficient ± SE |
|---|---|---|
| CHP1 | 89.9 ± 9.3 | 0.77 ± 0.12 |
| myr-CHP1 | 86.4 ± 8.9 | 0.94 ± 0.17 |
| CHP1/NHE1 | 2.32 ± 0.18 | 1.22 ± 0.15 |
| EF1m/NHE1 | 2.17 ± 0.39 | 0.98 ± 0.14 |
| EF3m/NHE1 | 2.89 ± 0.28 | 1.27 ± 0.55 |
| EF4m/NHE1 | 2.24 ± 0.26 | 0.76 ± 0.09 |

[a] The data shown in Figure 2 were fitted to the equation for equilibrium $^{45}Ca^{2+}$ binding as described in Experimental Procedures.

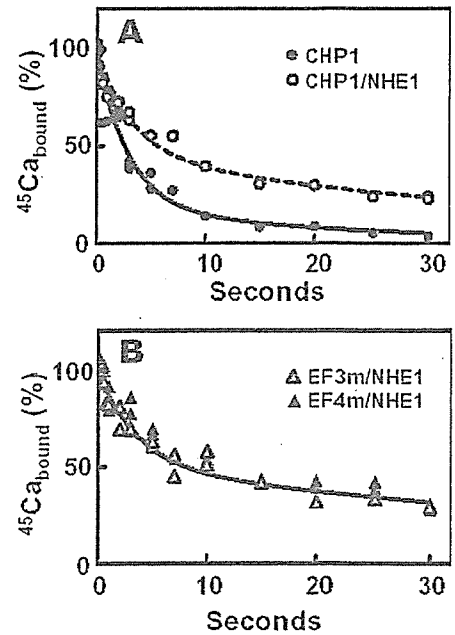


FIGURE 3: Time courses of $^{45}Ca^{2+}$ release from CHP1 proteins: (A) $^{45}Ca^{2+}$ release from CHP1 alone (●) or CHP1/NHE1 complex (○); (B) $^{45}Ca^{2+}$ release from EF3m/NHE1 (△) or EF4m/NHE1 complex (▲). CHP1 proteins or the complex of CHP1 variants with the NHE1 segment (aa 503−545) (0.1−0.2 mg/mL) were incubated for 1 h in a solution containing 50 $\mu$M $^{45}CaCl_2$, applied to Millipore filters, and washed with a solution containing EGTA. $^{45}Ca^{2+}$ remaining on the filters was measured.

maximal level of $^{45}Ca^{2+}$ binding (Figure 2A and Table 1). Interestingly, when CHP1 formed a complex with the NHE1 fragment, the binding affinity for $^{45}Ca^{2+}$ increased markedly (~40-fold, Figure 2A and Table 1). The extremely low apparent dissociation constant (~2 nM) deviates substantially from the physiological cytosolic $Ca^{2+}$ concentration of cells (0.1−10 $\mu$M). The maximal level of $Ca^{2+}$ binding on the complex again corresponded to ~2 mol of $Ca^{2+}$ bound/mol of CHP1. Mutation of either of $Ca^{2+}$ binding motifs EF3 or EF4, but not EF1, resulted in loss of approximately 1 mol of $^{45}Ca^{2+}$ bound to the complex (Figure 2C). On the other hand, $^{45}Ca^{2+}$ binding was completely blocked when the experiment was carried out using EF3m and EF4m proteins but without the NHE1 fragment (Figure 2B) or when two sites were simultaneously mutated (EF34m) (Figure 2C). Together, these results indicate that CHP1 binds two $Ca^{2+}$ ions, one at EF3 and the other at EF4.

To determine how complex formation increases the $Ca^{2+}$ binding affinity, we measured $^{45}Ca^{2+}$ release from CHP1 proteins by rapid filtration. As shown in Figure 3A, most of the $^{45}Ca^{2+}$ bound to CHP1 without the NHE1 fragment was released rapidly ($t_{1/2}$ = ~2 s). In contrast, $^{45}Ca^{2+}$ release from

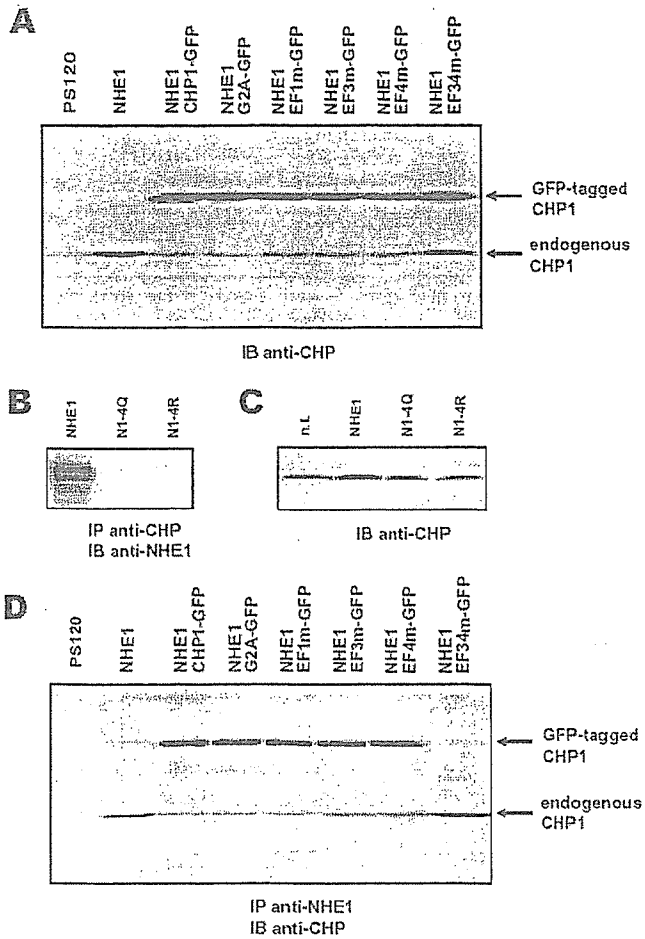


FIGURE 4: Expression of various GFP-tagged CHP1 proteins and their coimmunoprecipitation with NHE1. Panel A shows the expression level of GFP-tagged CHP1 and its variants (indicated at the top of the figure). Cell lysates (50 $\mu$g) from stable transfectants were subjected to SDS−PAGE, and expression of endogenous and exogenous CHP1 proteins were detected by immunoblotting (IB) with an anti-CHP1 antibody. A result for untransfected PS120 cells is shown in the first lane. Panel B shows coimmunoprecipitation of the wild-type or mutant (4Q and 4R) exchangers with endogenous CHP1. Lysates from cells stably expressing these exchangers were subjected to immunoprecipitation with anti-CHP1 antibody followed by immunoblotting with anti-NHE1 antibody. Panel C shows the expression level of endogenous CHP1 in cells expressing the wild-type or mutant NHE1s: n.t., no transfection. Panel D shows coimmunoprecipitation of CHP1 proteins with NHE1. Lysates from cells stably expressing various proteins were subjected to immunoprecipitation with anti-NHE1 antibody followed by immunoblotting with anti-CHP1 antibody. Note that in lanes from cells not transfected with GFP-tagged CHP1 (left two lanes), IgG protein bands were visible at the same positions as GFP-tagged CHP1.

CHP1 complexed with the NHE1 fragment ($t_{1/2} = \sim 7$ s) was much slower. A slow release of $^{45}Ca^{2+}$ also occurred in two mutant CHP1 proteins, EF3m and EF4m, complexed with the NHE1 fragment (Figure 3B), suggesting that $Ca^{2+}$ binds tightly to each EF hand.

*Effects of CHP1 Mutations on NHE1 Regulation.* To study the role of $Ca^{2+}$ binding in NHE1 regulation by CHP1, we transfected GFP-tagged CHP1 into cells expressing NHE1 and obtained cells stably coexpressing these proteins. The results indicated that GFP-tagged CHP1 and its mutant derivatives were highly coexpressed in NHE1 transfectants (Figure 4A). Interestingly, expression of NHE1 markedly increased the level of expression of the endogenous CHP1 (3.6-fold), while coexpression of various GFP-tagged CHP1 variants, with the exception of CHP1-EF34m-GFP, reduced it (Table 2).

Table 2: Relative Amounts of Expressed GFP-Tagged CHP1 and Endogenous CHP1

| transfected proteins | relative amount of GFP-tagged CHP1[a] | relative amount of endogenous CHP[b] |
|---|---|---|
| untransfected | | 1.00 ± 0.08 |
| NHE1 | | 3.63 ± 0.81[c] |
| NHE1 + CHP1-GFP | 1.00 ± 0.11 | 1.11 ± 0.13 |
| NHE1 + G2A-GFP | 1.08 ± 0.11 | 1.03 ± 0.16 |
| NHE1 + EF1m-GFP | 0.93 ± 0.06 | 1.07 ± 0.11 |
| NHE1 + EF3m-GFP | 0.97 ± 0.11 | 1.15 ± 0.16 |
| NHE1 + EF4m-GFP | 1.06 ± 0.07 | 1.09 ± 0.10 |
| NHE1 + EF34m-GFP | 0.94 ± 0.12 | 3.85 ± 0.45[c] |
| NHE1-4Q | | 1.02 ± 0.09 |
| NHE1-4R | | 1.03 ± 0.06 |

[a] The density of visualized protein bands on immunoblots (cf. Figure 4, panels A and C) is represented as values normalized according to the band density from cells expressing CHP1-GFP. Data are means ± SD ($n = 3$). [b] The band density is represented as values normalized according that from untransfected PS120 cells. Data are means ± SD ($n = 3$). [c] $P < 0.05$ versus control.

We further examined the effect of expression of CHP1 binding-defective NHE1 mutants 4Q and 4R on the amount of endogenous CHP. These mutant exchangers do not bind CHP1 as shown by coimmunoprecipitation studies (Figure 4B). The level of expression of the endogenous CHP1 did not increase on coexpression of these mutant exchangers (Figure 4B,C, Table 2). Thus, the amount of endogenous CHP1 in cells is highly dependent on expression of NHE1 and GFP-tagged CHP1.

Figure 4D shows the results for coimmunoprecipitation experiments using NHE1- and CHP1-specific antibodies to determine interactions of the expressed CHP1−GFP with NHE1. Anti-NHE1 antibody immunoprecipitated endogenous CHP1 from cells expressing NHE1. In cells coexpressing GFP−CHP1 and NHE1, the same antibody coimmunoprecipitated large quantities of GFP−CHP1 or its derivatives, and at the same time, the amount of immunoprecipitated endogenous CHP1 was markedly reduced. In cells coexpressing EF34m−GFP and NHE1, anti-NHE1 antibody coimmunoprecipitated the endogenous CHP1 but not exogenous GFP-tagged mutant CHP1, consistent with the findings of in vitro binding studies indicating that double mutation at EF3 and EF4 impairs the interaction of CHP1 with NHE1.

We next examined the subcellular localization of GFP-tagged CHP1. As reported previously (*12*), the GFP-tagged CHP1 is localized in the plasma membrane in cells coexpressing NHE1 (Figure 5A). Consistent with the in vitro binding data (Figure 1B), the GFP fluorescence was observed in the plasma membrane in cells coexpressing GFP-tagged CHP1 mutants except EF34m with NHE1 (Figure 5A; data not shown for G2A and EF1m). These results, together with the data from coimmunoprecipitation experiments, indicate that the endogenous CHP1 bound to NHE1 was efficiently replaced by expressed GFP-tagged wild-type or CHP1 mutants. However, the double mutant EF34m was not localized at the plasma membrane (Figure 5A) because of the weak interaction of this mutant protein with the juxtamembrane region of NHE1. We observed that GFP fluorescence was still observed in the plasma membrane after addition of phorbol ester, serum, thrombin, lysophosphatidic

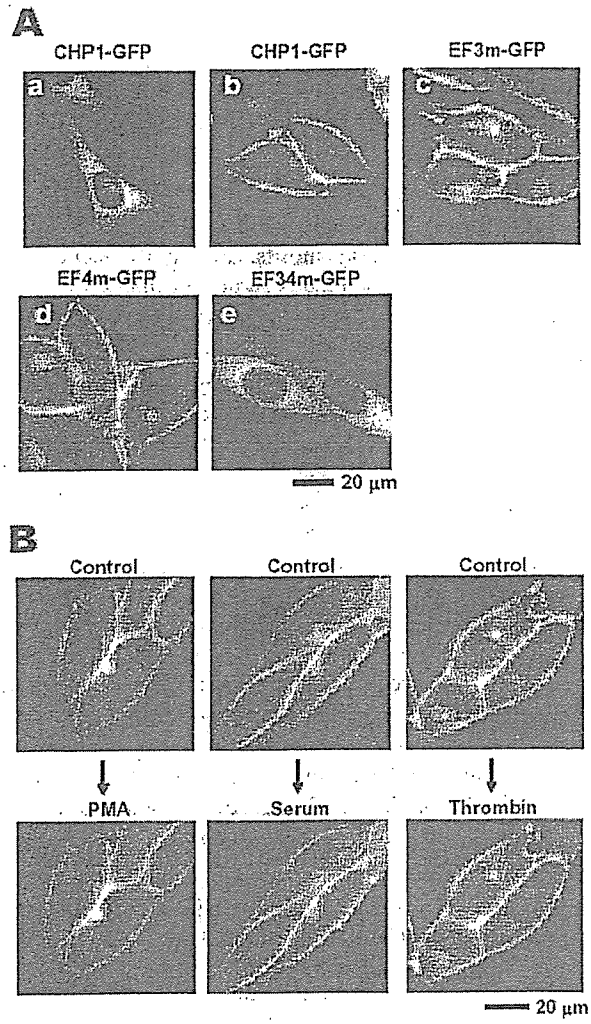


FIGURE 5: Subcellular localization of GFP-tagged CHP1: (A) subcellular localization of GFP-tagged wild-type CHP1 (a, b), EF3m (c), EF4m (d), and EF34m (e) expressed in PS120 cells (a) or in their stable transfectants of the wild-type NHE1 (b–e); (B) effect of various agents on the subcellular localization of the wild-type GFP-tagged CHP1 in NHE1 transfectants. Cells were placed in serum-free Dulbecco's modified Eagle's medium without phenol red for 5 h, and then 1 $\mu$M PMA, 10% serum, or 2 units/ml thrombin were added. GFP fluorescence was observed under a fluorescent microscope equipped with a CoolSNAP imaging system (RS Photometrics) before (control) and 20 min after addition of the various agents.

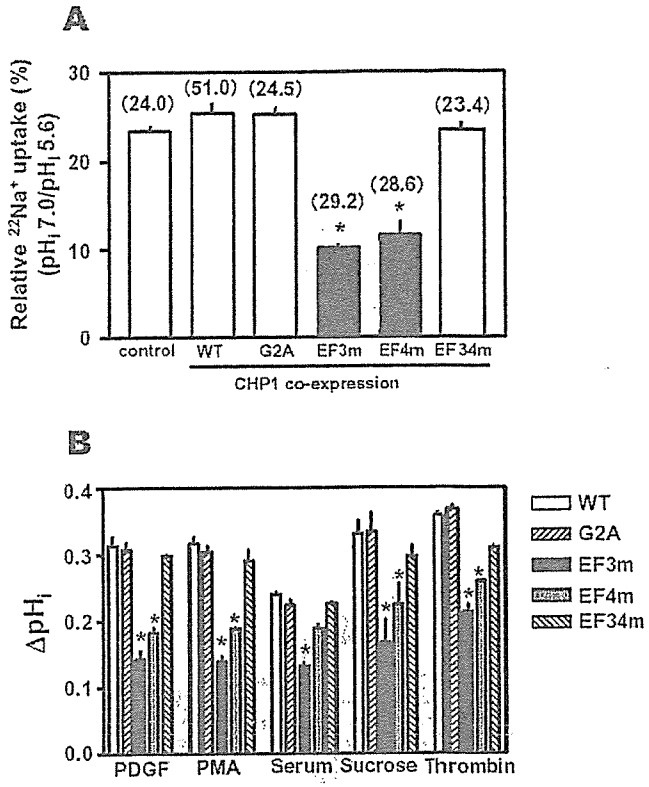


FIGURE 6: Exchange activity and regulation of NHE1 transfectants expressing various CHP1 mutants. Panel A shows ratios of EIPA-sensitive $^{22}Na^+$ uptake activities of cells coexpressing wild-type NHE1 and various CHP1 mutants at pH$_i$ 7.0 and 5.6. Numbers (nmol/mg/min) in parentheses represent $^{22}Na^+$ uptake activity at pH$_i$ = 5.6. Control cells were not transfected with CHP1 but stably expressing NHE1. Data are means ± SD ($n$ = 3; *, $P$ < 0.05 versus cells not expressing exogenous CHP1). Panel B shows changes in pH$_i$ measured using the [$^{14}$C]benzoic acid equilibration method. The cells coexpressing NHE1 and various CHP1 variants were stimulated for 15 min at 37 °C with 10 ng/mL PDGF-BB, 1 $\mu$M PMA, 10 $\mu$g/mL lysophosphatidic acid, or 200 mM sucrose (hyperosmotic stress). Data are means ± SD ($n$ = 6; *, $P$ < 0.05 versus cells expressing wild-type CHP1).

acid, or PDGF-BB, which are all known to activate the exchange activity (Figure 5B, data not shown for some experiments). We also found that the plasma membrane localization of GFP fluorescence did not change upon addition of metabolic inhibitors (2-deoxyglucose plus oligomycin) that cause cell ATP depletion, thus inhibiting exchange activity (data not shown). Furthermore, we found no changes in the plasma membrane localization of GFP-tagged CHP1 mutants EF3m and EF4m after these various treatments (data not shown). These observations suggest that CHP1 is tightly associated with NHE1 in the plasma membrane and that this interaction is not affected by various stimuli.

All the cells expressing CHP1–GFP or its mutant derivatives exhibited high $Na^+/H^+$ exchange activity. The $^{22}Na^+$ uptake activity in cells clamped at acidic pH$_i$ (5.6) by the $K^+$/nigericin technique was in the range of 20–50 nmol/mg/min (data not shown). We compared the $^{22}Na^+$ uptake activities in cells expressing various CHP1 variants in the physiological pH$_i$ range. As shown in Figure 6A, the ratio of $^{22}Na^+$ uptake at pH$_i$ 7.2–5.6 was not significantly altered by expression of wild-type CHP1. Although a previous study (*11*) indicated that overexpression of CHP1 inhibits the NHE1 activity in the presence of serum, we observed no such CHP1-induced inhibition of the exchange activity. The reason for this discrepancy is unknown. Unlike the wild-type CHP1, the $^{22}Na^+$ uptake ratio was significantly reduced by EF3 or EF4 mutants. Consistent with this finding, we observed that mutations of EF3 or EF4 significantly reduced the cytoplasmic alkalinization in response to PDGF-BB, thrombin, phorbol ester, serum, or hyperosmotic stress (sucrose) (Figure 6B). These observations suggest that mutation of EF3 or EF4 partly impairs the regulation of NHE1 by reducing pH$_i$ sensitivity. In contrast, double mutation (EF34m) of CHP1 at EF3 and EF4 did not reduce the $^{22}Na^+$ uptake ratio or cytoplasmic alkalinization (Figure 6A,B), consistent with the finding that this mutant CHP1 is not able to replace the endogenous CHP1 because of its weak interaction with NHE1. Finally, mutation of the myristoylation site (G2A) or EF1 did not affect pH$_i$-dependent regulation of NHE1.

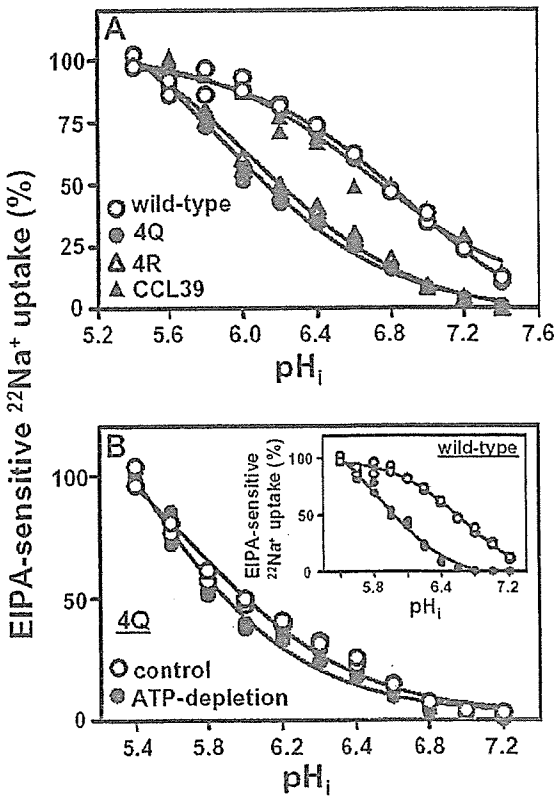


FIGURE 7: $pH_i$ dependence of exchange activity in cells expressing some NHE variants. Panel A shows the $pH_i$ dependence of $^{22}Na^+$ uptake in PS120 cells expressing wild-type NHE1 or CHP1 binding-defective mutants 4Q and 4R and CCL39 fibroblastic cells (the parental cell line of PS120). $pH_i$ was clamped at various values with $K^+$/nigericin. The maximal EIPA-sensitive $^{22}Na^+$ uptake activity measured at $pH_i = 5.4$ was high in cells expressing wild-type NHE1 (~50 nmol/mg/min), while it was lower but similar in cells expressing 4Q or 4R or in CCL39 cells (4.2, 4.2, or 4.1 nmol/mg/min, respectively). Data were normalized according to the maximal activity at $pH_i = 5.4$. Panel B shows the effects of ATP depletion on $pH_i$ dependence of exchange activity in cells expressing 4Q or wild-type NHE1 (inset). Cells were depleted of ATP by treatment with the metabolic inhibitors 2-deoxyglucose (5 mM) and oligomycin (2 μg/mL). Data were normalized according to the maximal activity at $pH_i = 5.4$.

*Properties of NHE1 Mutants Lacking CHP1 Binding.* As described above, mutations of CHP1 partly impair $pH_i$-dependent regulation of NHE1. Therefore, it is of interest to determine how CHP1 binding affects the $pH_i$ sensitivity of NHE1. Previously, we described two CHP1 binding-defective mutant exchangers, 4Q or 4R, in which $Phe^{526}$, $Leu^{527}$, $Leu^{530}$, and $Leu^{531}$ of NHE1 were replaced by four glutamine or arginine residues, respectively (*12*) (see Figure 4B). In this study, by using extensive $H^+$-killing selection, we obtained cells overexpressing 4Q or 4R and exhibiting relatively high activity (~4 nmol/mg/min at $pH_i$ 5.4), thus allowing reliable measurement of the $pH_i$ dependence of $^{22}Na^+$ uptake. As shown in Figure 7A, these mutations caused a marked acidic shift in the $pH_i$ dependence (Figure 7A). As a control, we confirmed that CCL39 cells (the parental cell line of PS120) that exhibit exchange activity ($V_{max}$) comparable to 4Q or 4R show a $pH_i$ dependence of exchange similar to that of PS120 cells overexpressing NHE1. In cells expressing these mutant exchangers, ATP depletion did not change the $pH_i$ sensitivity of $^{22}Na^+$ uptake (Figure 7B). In addition, cytoplasmic alkalinization in response to extracellular stimuli, such as thrombin, PDGF-BB, hyperosmolarity, LPA, and PMA, was not observed in cells expressing 4Q or 4R (data not shown), consistent with the finding that these mutants exhibit an acidic shift of $pH_i$ dependence.

## DISCUSSION

In this study, we examined the role of CHP1, particularly its EF-hand $Ca^{2+}$ binding motifs, in the $pH_i$-dependent regulation of NHE1. Our results indicated that a $Ca^{2+}$ ion binds to each of EF3 and EF4 in CHP1 with an overall apparent $K_d$ of ~90 nM and a Hill coefficient of ~1.0 (Table 1). This $Ca^{2+}$ binding affinity was close to that of another family member, CaN-B (apparent $K_d \approx 70$ nM) (*36*), although the apparent $K_d$ values for $Ca^{2+}$ in other EF-hand $Ca^{2+}$ binding proteins vary widely (0.01−10 μM) (*36*−*39*). Although CHP1 potentially has four $Ca^{2+}$ binding motifs, the two ancestral sites EF1 and EF2 do not bind $Ca^{2+}$. This is in sharp contrast to CaN-B in which all four EF-hand motifs are able to bind $Ca^{2+}$, although the two N-terminal sites, EF1 and EF2, have lower affinity for $Ca^{2+}$ than the C-terminal sites, EF3 and EF4 (*36*). Intriguingly, the $Ca^{2+}$ affinity of CHP1 increased markedly upon complex formation with the NHE1 fragment (aa 503−545). Consistent with this finding, $^{45}Ca^{2+}$ release from the complex was much slower than that from CHP1 alone. The extraordinarily high affinity of CHP1 for $Ca^{2+}$ (~2 nM) suggests that the CHP1/NHE1 complex always contains two $Ca^{2+}$ ions under physiological conditions.

The high affinity for $Ca^{2+}$ was also observed in mutant CHP1 proteins EF3m and EF4m, which have a single $Ca^{2+}$ binding site, complexed with the NHE1 fragment. Increases in the affinity for $Ca^{2+}$ by interaction with target proteins have also been reported for other $Ca^{2+}$ binding proteins. For example, the $Ca^{2+}$ binding affinity for calmodulin was increased 16- to 38-fold upon interaction with myosin light chain kinase (*40*), 2.6-fold with myristoylated alanine-rich protein kinase C substrate peptide (*41*), and 75-fold with the calmodulin binding peptide in CaN-A (*36*). CHP1 was reported to interact with other proteins, such as microtubules (*25*), CaN-A (*24*), DRAK2 (*26*), and KIF1Bβ2 (*27*), as well as members of the NHE1 family. Therefore, interaction with these proteins may also modify the $Ca^{2+}$ binding affinity of CHP1.

Although mutation of CHP1 at either EF3 or EF4 impaired binding of 1 mol of $Ca^{2+}$, it did not appear to affect the interaction of CHP1 with NHE1 as shown by in vitro binding of these mutant proteins, coimmunoprecipitation, and the plasma membrane localization of GFP-tagged CHP1. Therefore, these mutations do not appear to induce marked structural distortions. However, double mutation (EF34m) at both EF3 and EF4 impaired the interaction of CHP1 with NHE1. Consistent with this finding, $Ca^{2+}$ removal by EGTA from the wild-type CHP1 reduced the interaction with NHE1 in a pull-down assay through the amyrose resin column (data not shown). Thus, the tight association of NHE1 with CHP1 requires binding of at least one $Ca^{2+}$ on either EF3 or EF4. Furthermore, it should be noted that the effect of double mutation (EF34m) on regulation of NHE1 cannot be properly analyzed in cells that express endogenous CHP1.

We found that expression of NHE1, but not the CHP1 binding-deficient mutant derivatives 4Q and 4R, significantly

increased the amount of endogenous CHP1. However, coexpression of GFP-tagged CHP1 proteins (wild-type, EF3m, and EF4m) preserving the strong interaction with NHE1 greatly reduced the amount of endogenous CHP1. Thus, the amount of endogenous CHP1 in cells is strongly dependent on the number of available CHP1 binding sites provided from NHE1. Although the precise reason for this is unknown, it is likely that interaction with target proteins is required for stable expression of CHP1. That is, dissociation from the target proteins may promote CHP1 degradation.

In this study, we found that CHP1 binding-defective mutants of NHE1 (4Q and 4R) caused a marked acidic shift in the $pH_i$ dependence of $Na^+/H^+$ exchange activity and completely impaired ATP depletion-induced inhibition and cytoplasmic alkalinization in response to various stimuli. As we reported previously (*32*), not only mutation of the CHP1 binding region, but also deletions of different regions in the amino-terminus (subdomain I, amino acids 515−595) of the NHE1 cytoplasmic domain also markedly reduced $pH_i$ sensitivity. Thus, subdomain I with bound CHP1 appears to be a key structure that permits the putative "pH-sensor" to maintain a physiologically relevant conformation.

We found that mutation of EF3 or EF4 in CHP1 significantly reduced the $Na^+/H^+$ exchange activity in the physiological neutral $pH_i$ range and reduced the cytoplasmic alkalinization in response to various extracellular signals by decreasing the $pH_i$ sensitivity of NHE1. Thus, mutation of each EF-hand in CHP1 somehow affects the $pH_i$-sensing of NHE1, although we could not evaluate the function of the double mutant CHP1 (EF34m) because of its weak interaction with NHE1. We found that EF3m, EF4m, and EF34m proteins migrated slowly on SDS−PAGE, suggesting that significant conformational changes of CHP1 occur upon mutation of each EF-hand. Such conformational changes appear to be due to removal of $Ca^{2+}$ rather than the amino acid substitution itself, because incubation with EGTA resulted in similar slow migration of the wild-type CHP1 on SDS−PAGE (data not shown). Thus, the bound $Ca^{2+}$ may play an important role in maintaining the CHP1 structure, thereby preserving the physiological $pH_i$ sensitivity of NHE1.

According to the structural model of CHP1 deduced from the three-dimensional structure of CaN-B (*43*), EF-hand $Ca^{2+}$ binding motifs would be located on the surface opposite the side where CHP1 binds to NHE1. It is likely that the surface of CHP1 with tightly bound $Ca^{2+}$ controls the $pH_i$-sensing by interacting with other region(s) of NHE1. We observed that the $pH_i$ sensitivity of NHE1 was markedly reduced by insertion of one amino acid residue (alanine) just to the N-terminal side (position aa 504 or 508) of the CHP1 binding site of NHE1, while the CHP1 binding ability was preserved (our unpublished observations). Therefore, the correct spatial orientation of CHP1 would be important for regulation of NHE. Recently, we reported that mutation of $Arg^{440}$ in intracellular loop 5 (IL5), which connects transmembrane helices 10 and 11, markedly reduces the $pH_i$ sensitivity of NHE1 (*44*). Thus, IL5 may interact with the CHP1 surface with tightly bound $Ca^{2+}$.

Many EF-hand $Ca^{2+}$ binding proteins are known to regulate the functions of their target proteins in response to cytosolic $Ca^{2+}$ mobilization. However, it is unlikely that CHP1 functions as such a $Ca^{2+}$ sensor in the regulation of NHE1 because the affinity for $Ca^{2+}$ ($K_d$ = ~2 nM) for the CHP1/NHE1 complex differs substantially from the range of intracellular $Ca^{2+}$ concentrations (0.1−10 $\mu$M). Instead, two EF-hand motifs of CHP1 together with tightly bound $Ca^{2+}$ would serve as structurally important elements for preserving the normal function of NHE1, as discussed above. Such a structural role has also been suggested in the C-terminal EF-hand motifs in CaN-B (*42*) and in CaM (*41*). On the other hand, we reported previously that CaM interacts in a $Ca^{2+}$-dependent manner with the middle of the cytoplasmic domain of NHE1, which in the unstipulated state serves as an auto inhibitory domain decreasing the $pH_i$ sensitivity of NHE1 (*14*, *15*). The interaction of NHE1 with CaM is strictly $Ca^{2+}$-dependent, although it is much weaker than that with CHP1 (*14*). Previously, we proposed that NHE1 may be activated by $Ca^{2+}$-dependent interaction of CaM in response to $Ca^{2+}$-mobilizing signals (*15*). Our previous (*14*, *15*) and several recent reports (*45*−*48*) reinforced the idea that CaM serves as an important regulatory protein in activation of NHE1 in response to hyperosmotic stress or $Ca^{2+}$-mobilizing agonists. NHE1 thus appears to be dually regulated by two $Ca^{2+}$ binding proteins, CHP1 and CaM, similar to CaN-A. The former would preserve the physiological $pH_i$ sensitivity of NHE1, whereas the latter would play a role in sensing cytosolic $Ca^{2+}$.

In summary, our current results suggest that the interaction of CHP1 with NHE1 is crucial for preserving the physiological $pH_i$ sensitivity of NHE1 and that tightly bound $Ca^{2+}$ serves as an important structural element that is required for this role. The significant effects of mutations in EF-hands on NHE1 regulation prompted us to generate a more efficient dominant negative mutant CHP1. In addition, the functional difference between CHP1 and CHP2, which we reported recently (*13*), provides important information for identification of the critical residues of CHP1. Further studies including analyses of the functions of mutated or chimerical CHP1 and determination of the crystal structure of CHP1/NHE1 complex are required to elucidate the molecular mechanism of CHP regulation of NHE1 and other NHE family members.

## REFERENCES


1. Wakabayashi, S., Shigekawa, M., and Pouysségur, J. (1997) Molecular physiology of vertebrate $Na^+/H^+$ exchangers, *Physiol. Rev. 77*, 51−74.
2. Orlowski, J., and Grinstein, S. (1997) $Na^+/H^+$ exchangers of mammalian cells, *J. Biol. Chem. 272*, 22373−22376.
3. Counillon, L., and Pouysségur, J. (2000) The expanding family of eucaryotic $Na^+/H^+$ exchangers, *J. Biol. Chem. 275*, 1−4.
4. Sardet, C., Franchi, A., and Pouysségur, J. (1989) Molecular cloning, primary structure, and expression of the human growth factor-activatable $Na^+/H^+$ antiporter, *Cell 56*, 271−280.
5. Orlowski, J., Kandasamy, R. A., and Shull, G. E., (1992) Molecular cloning of putative members of the Na/H exchanger gene family, *J. Biol. Chem. 267*, 9331−9339.
6. Tsé, C.-M., Brant, S. R. Walker, M. S., Pouysségur, J., and Donowitz, M. (1992) Cloning and sequencing of a rabbit cDNA encoding and intestinal and kidney-specific $Na^+/H^+$ exchanger isoform (NHE-3), *J. Biol. Chem. 267*, 9340−9346.
7. Numata, M., Petrecca, K., Lake, N., and Orlowski, J. (1998) Identification of a mitochondrial $Na^+/H^+$ exchanger, *J. Biol. Chem. 273*, 6951−6959.
8. Numata, M., and Orlowski, J. (2001) Molecular cloning and characterization of a novel ($Na^+$, $K^+$)/$H^+$ exchanger localized to the *trans*-Golgi network, *J. Biol. Chem. 276*, 17387−17394.
9. Baird, N., Orlowski, J., Szabo, E. Z., Zaun, H. Schultheis, P. J., Menon, A. G., and Shull, G. (1999) Molecular cloning, genomic